

Salinity and density modifications of synthetic H₂O and H₂O–NaCl fluid inclusions in re-equilibration experiments at constant temperature and confining pressure

Ronald J. Bakker*, Gerald Doppler

Department of Applied Geological Sciences and Geophysics, Montanuniversitaet Leoben, Austria

ARTICLE INFO

Article history:

Received 16 July 2015

Received in revised form 15 January 2016

Accepted 20 January 2016

Available online 21 January 2016

Keywords:

Fluid inclusions

H₂O–NaCl

Re-equilibration

Diffusion

Volume changes

ABSTRACT

Experiments have been performed to elucidate post-entrapment modifications of natural fluid inclusions. Synthetic H₂O and H₂O–NaCl fluid inclusions in quartz were re-equilibrated at 599.7–600.7 °C and 332.6–338.3 MPa in hydrothermal autoclaves, and subjected to H₂O fugacity gradients at similar temperature and hydrostatic pressure conditions to those of the original syntheses. Individual inclusions in specific assemblages were analyzed in detail, i.e. size, shape, depth, homogenization and ice-dissolution temperatures, before and after the re-equilibration experiments. Accurate loading and unloading of the samples along isochoric *T*–*p* paths require monitoring the temperature at the sample within the autoclaves. Multiple loading and unloading of the samples along these paths do not affect the properties of fluid inclusions. Synthetic H₂O fluid inclusions are not modified after re-equilibration in a pure H₂O fluid, but reveal significantly higher homogenization temperatures after re-equilibration in 20 mass% NaCl solution. Synthetic NaCl–H₂O fluid inclusions with 10, 16.3 and 19.8 mass% NaCl reveal higher salinities after re-equilibration in a pure H₂O fluid, and highly variable homogenization temperatures: positive as well as negative modifications. The magnitude of modifications indicates that two processes must have operated simultaneously to obtain the observed homogenization and dissolution temperatures in individual inclusions: (1) preferential H₂O loss via diffusion; and (2) total volume loss by diffusion of quartz into the former inclusion volume. These processes are inconsistent with the expected H₂O diffusion into inclusions according to the applied fugacity gradients in the experimental setup. These simultaneously operating processes are suggested to be the main modification method of natural fluid inclusions in a variety of experimental settings and in geological environments.

© 2016 Elsevier B.V. All rights reserved.

1. Introduction

Fluid inclusions are important indicators of rock forming conditions (e.g. Samson et al., 2003), and knowledge about the possibility of post-entrapment modifications of fluid inclusion properties is of major importance to the interpretation of natural fluid inclusion. Modifications of fluid inclusions in natural environments were discussed by prior authors, e.g. Barker (1995), Küster and Stöckhert (1997), Audétat and Günther (1999), and Ayllón et al. (2003). The general argumentation is mainly based on textural analyses of individual fluid inclusions and a large variation in homogenization and dissolution temperatures of aqueous and gaseous phases in specific fluid inclusion assemblages. These studies do not provide information about processes and driving forces that may modify fluid inclusion properties, and do not identify the parameters involved in diffusion and deformation. The importance of diffusion in fluid modifications in inclusions was illustrated in experimental studies by Bakker (2009) and Doppler et al. (2013), at

controlled temperature, hydrostatic pressure, and fluid composition conditions.

Fluid properties of fluid inclusion assemblages with pure H₂O and H₂O–NaCl mixtures are investigated in the present study, before and after re-equilibration at specific *T*–*p* conditions. Each individual inclusion in these assemblages is analyzed before the re-equilibration experiment, then located after the experiment and measured again. Water and salt, in general NaCl, are major components in natural fluids that are observed in natural fluid inclusions in most types of rocks (e.g. Roedder, 1984). These inclusions are often hosted by quartz, which is a nominally anhydrous mineral, i.e. it does not contain H₂O or related chemical compounds in a regular crystal lattice. However, the amount of water in quartz is defined by structural OH groups and nano-scale water clusters (crystal defects), in addition to fluid inclusions (e.g. Johnson, 2006; Bakker, 2009; and references therein). NaCl is usually restricted to fluid inclusions, or incorporated as single salt crystals (solid inclusions) within quartz (e.g. Bakker and Elburg, 2006).

Experiments in this study are performed exclusively at constant temperature and initial confining pressure conditions, i.e. 600 °C and 337 MPa, within the α-quartz stability field (see also Doppler and Bakker, 2014), for

* Corresponding author.

E-mail address: bakker@unileoben.ac.at (R.J. Bakker).

evaluating only the effect of H_2O - and NaCl -fugacity gradients on fluid inclusion modification. Bakker (2009) and Doppler et al. (2013) showed that such gradients in water fugacity (or chemical potential) cause diffusion through a homogeneous anhydrous medium such as quartz. Therefore, water diffusion is expected in the form of molecular H_2O through the quartz lattice in our experiments. Diffusion of water-related OH^- ions must be balanced with the counter ion H^+ or H_3O^+ to ensure electrical neutrality. Experimental runtime varies from 5, 19, to 40 days to investigate time-dependent processes, such as diffusion.

Experimental re-equilibration studies on synthetic pure H_2O and H_2O – NaCl fluid inclusions in natural quartz were presented by various authors (Sterner and Bodnar, 1989; Sterner et al., 1995; Vityk and Bodnar, 1995, 1998). These studies reveal abundant deficiencies to justify a new approach in this work. The potential individual parameters that may modify fluid inclusions were not completely identified in previous work. For example, the α – β quartz phase transition results in a density loss of synthetic H_2O fluid inclusions (Doppler and Bakker, 2014). The experiments of Vityk and Bodnar (1995, 1998) were performed exactly at α – β quartz phase transition conditions, whereas parts of the experiments of Sterner and Bodnar (1989) and Sterner et al. (1995) were performed in the β quartz stability field. However, the phase transition was not considered as a process to modify fluid inclusions. Sterner and Bodnar (1989) re-equilibrated pure H_2O synthetic fluid inclusions in a 20 mass% NaCl aqueous solution with accompanying large gradients in both pressure and H_2O fugacity, up to 400 MPa and 438 MPa, respectively. These large gradients must provoke H_2O diffusion and deformation of fluid inclusions at experimental conditions, as evidenced by e.g. Doppler et al. (2013), but only changes in total inclusion volume were suggested to be the cause of density modifications by Sterner and Bodnar (1989). In contrast to these results, Sterner et al. (1995) concluded that H_2O diffusion is the process that modifies fluid inclusions at constant temperatures and confining pressures. They re-equilibrated highly saline aqueous inclusions (e.g. 57 mass% NaCl) in argon and pure H_2O at T – p conditions within the β quartz stability field. They only identified modifications of NaCl dissolution temperatures. Homogenization temperatures were not given and changes in T_h were only rarely indicated for some inclusion assemblages. The amount of H_2O loss or gain can be calculated from the change in NaCl dissolution temperatures, but this was always inconsistent with the corresponding change in T_h in Sterner et al. (1995), if water diffusion is the sole process of modification. Another enigmatic result of this study was that the experiments with higher gradients in H_2O fugacity reveal lower modifications in dissolution temperatures. Moreover, modifications of natural fluid inclusions were more intense at lower temperatures. Both observations cannot be explained with diffusion. Moreover, the results of that study were not sufficiently elucidated, and the incomplete presentation of data does not allow an unambiguous interpretation of these experiments. The experimental setup in Vityk and Bodnar (1995, 1998) does not allow a direct comparison of individual fluid inclusions before and after re-equilibrations, but was based on a bulk analysis of T_h values in distribution diagrams. The stepwise unloading of these experiments may perhaps cause the formation of multiple generations of fluid inclusions with a variety of inclusion densities, and each generation may therefore be subject to different re-equilibration conditions. That study can only illustrate the average change of a fluid inclusion assemblage, but it does not reveal any information about the effect of diffusion, deformation or α – β quartz phase transition on the properties of individual fluid inclusions. Modifications of homogenization temperatures do not provide sufficient information to interpret re-equilibration processes.

2. Experimental procedure

2.1. Hydrothermal laboratory

The experiments were carried out in the hydrothermal laboratory at the Montanuniversität Leoben (Austria). The laboratory provides a

high temperature–pressure apparatus that enables conditions of maximum 1 GPa confining pressure and 700 °C. The device is constructed with 10 Nimonic IOS/René 41 autoclaves (Ni–Cr alloy) in a vertical position, with a cold-seal system (Doppler, 2014; Kerrick, 1987). Argon was used as pressure medium that was compressed by a high-pressure pump system (Sitec). Pressure transducers register pressure with a variation of 2 MPa during the experiments. The transducers were calibrated up to 700 MPa with a Heise dial gauge with an accuracy of 0.015% of reading. External furnaces induced the appropriate temperature conditions. The temperature was measured by an internal thermocouple (NiCr–Ni, Type “K”) that allowed direct monitoring and recording of the sample temperature with an uncertainty of 0.1 °C. Temperature during the experimental run was stabilized within 2 °C. The internal thermocouple allows direct control of the experimental temperature conditions during loading and unloading according to specific fluid isochores. Experimental confining pressure and temperature were continuously logged by a computerized system. Each experiment in the present study, both synthesis and the complementary re-equilibration, was intended to be performed exclusively under identical conditions without any gradients in temperature and initial pressure or deviatoric stress.

The units and symbols of quantities such as fractions that are used in this study are strictly according to SI (Bakker, 2011). The use of “weight fraction” is omitted because it is an erroneous label for mass fraction (symbol “w”). Amount of substance fraction has the symbol “x” and is also known as “mole fraction”. However, a unit name (e.g. mole) should not be confused with a physical quantity.

2.2. Fluid inclusion synthesis

Fluid inclusions were synthesized according to the crack-healing method (e.g. Bodnar and Sterner, 1987). Natural inclusion-free Brazilian quartz crystals were used as starting material. Cores with a length of approximately 1 cm and a diameter of 2.75 mm were drilled along the c -axis of the quartz crystal. These cores were partially cracked by thermal shock after heating to 400 °C. Arc-welded Au-capsules were used as containers which were loaded with the cracked quartz core and pure de-ionized H_2O , 19.8 mass% NaCl , 16.3 mass% NaCl , or 10.0 mass% NaCl (sodium chloride, CAS-Nr. 7647-14-5, >99.8%, Carl Roth GmbH). The Au-capsules have a wall thickness of 0.5 mm, and an inner diameter of 3 mm (Ögussa GmbH). The initial setup of the Au-capsule is illustrated in Fig. 1 and Table 1. The Au-tubes were first loaded with a fluid after welding the bottom end of the tubes, and subsequently loaded with a small quartz rod on top of that fluid. The relatively long walls of the top part of the Au-tube were pressed together to reduce the initial total volume, and to facilitate final welding of the upper end of the tubes. The total mass of loaded fluid (Table 1) was selected not to exceed the maximum amount that the welded Au-capsule can contain at experimental conditions, without the development of an internal overpressure that may damage (rupture) the Au-capsule. For example, the maximum molar volume of the aqueous fluid in experiment GMR-004d is $41.36 \text{ cm}^3 \cdot \text{mol}^{-1}$ according to the given total volume of the Au-capsule (0.1205 cm^3).

At the start of each experiment, a small external hydrostatic Argon pressure of 10 to 30 MPa was applied to the Au-capsules, which resulted in collapsing the capsule and further reducing the total volume that was accessible to the loaded fluid. The expansibility of the fluid during the run-up procedure and during peak experimental conditions inflated the capsules to 45–85% of the maximum available volume due to the flexibility of the Au-walls at high temperatures and pressures, until confining pressure conditions were reached, equal to the external Argon pressure medium. The induced cracks entrapped the loaded fluid by fracture-healing processes during the synthesis experiment. Experimental T – p conditions of each experiment are given in Table 2. Loading and unloading the experiments were performed approximately along specific isochores of the entrapped fluid (Fig. 1) to prevent any stress

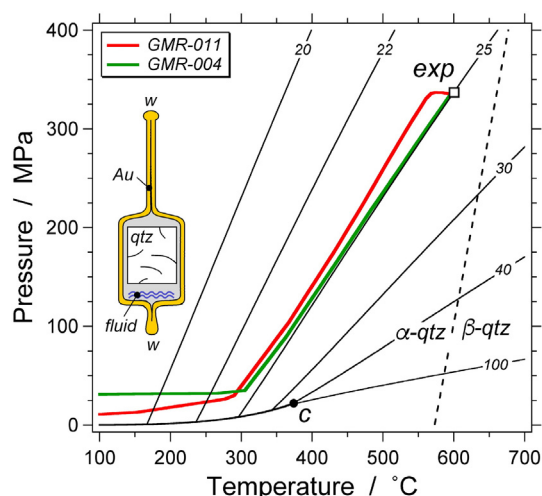


Fig. 1. Experimental T - p conditions of loading procedures of the initial synthesis GMR-004 and GMR-011, based on the computerized logging-system of the hydrothermal laboratory. Unloading and complementary re-equilibration experiments are performed along similar T - p trajectories. Thin solid lines are isochores of pure H_2O (numbers in $cm^3 \cdot mol^{-1}$) calculated with Haar et al. (1984). C is the critical point of pure H_2O , i.e. the end point of the liquid-vapor curve. exp is the location of experimental pressure and temperature, the size of the symbol reflects the variability in these conditions. The dashed line illustrates the α - β phase transition of quartz. The experimental set-up of an Au-capsule is schematically illustrated in this diagram. The cracked quartz core (qtz) is positioned within the Au-capsule in addition to a loaded fluid. The capsule is welded at the top and the bottom part (w). See text for further details.

that could cause cracking and deformation of the quartz around inclusions due to internal fluid over- or under-pressure. Duration of loading and unloading paths varied between 60 and 90 min. The synthesis experiments were carried out with a run-time of 454.3 to 462.4 h (approximately 19 days). The quartz cores were cut into approximately 0.5 mm thick disks, which were then polished on both sides to determine morphological, volumetric and microthermometric properties of the original fluid inclusions (Appendix).

2.3. Fluid inclusion re-equilibration

The same quartz disks were used again for re-equilibration experiments at similar temperature and confining pressure conditions (Table 2). Two quartz rods, one below and one above the relatively fragile analyzed quartz disk with synthetic fluid inclusions were placed in a

Table 1
Setup of the Au-capsules before experimentation in the initial synthesis experiments (GMR) and corresponding re-equilibration experiments (R).

Experiment	Length capsule ^a	Loaded fluid ^b	Total volume ^c	Min. density ^d	Max. V_m ^e
GMR-004d, g	2.8	0.05250	0.1205	0.4355	41.36
R-004d	2.7	0.05535	0.1182	0.4683	44.65
R-004g	3.3	0.09068	0.1782	0.5089	35.47
GMR-005a, b, c	2.7	0.07822	0.1480	0.5284	39.50
R-005c	3.4	0.06804	0.1908	0.3566	50.52
R-005a	2.7	0.07917	0.1302	0.6279	29.63
R-005b	2.7	0.07659	0.1250	0.6364	29.41
GMR-011a	3.4	0.06965	0.2010	0.3464	55.88
R-011a	3.5	0.07224	0.1949	0.3706	48.61
GMR-014a	3.4	0.07724	0.2028	0.3809	53.30
R-014a	3.4	0.07595	0.1981	0.3833	47.00

^a Length of Au-capsule (in cm).

^b Mass of loaded fluid (in g).

^c The maximum total volume of the Au-capsule available for the loaded fluid (in cm^3), corrected for the presence of a quartz rod.

^d The minimum density of the loaded fluid in the Au-capsule if the total volume is completely available (in $g \cdot cm^{-3}$).

^e The corresponding maximum molar volume (in $cm^3 \cdot mol^{-1}$).

gold capsule to prevent any damages during the re-equilibration experiment. Pure H_2O and an aqueous mixture of 20.0 mass% NaCl were added to the gold capsules in various experiments. Loading and unloading of the pressure vessels were performed again along the specific isochore of the entrapped fluid with the intention to prevent any fluid over- or underpressure within the inclusions and to obtain the same experimental temperature and confining pressure. Re-equilibration experiments were carried out with varying run-times: 120.4 h (5 days), 458.1–462.5 h (19 days) and 959.8–961.6 h (40 days). After the re-equilibration experiments dissolution temperature of ice (salinity), homogenization temperature (density) and inclusion morphology (two-dimensional analysis) were compared to their initial values in the synthesized fluid inclusions (Appendix).

2.4. Optical analysis and microthermometry

Each quartz disk was investigated by microscopic examinations with an optical microscope Olympus BX60. Up to 100 fluid inclusions were photographed for analyzing shape, size and identification purposes (Appendix). The distance of each fluid inclusion to the crystal surface was measured by focusing the inclusions with adjusting the z -direction of the microscope stage. Morphological aspects of fluid inclusions, i.e. (1) size and (2) shape were characterized by tracing digitally the outside edges of the inclusions in two-dimension images at room temperature according to the method described by Bakker and Diamond (2006). Homogenization and dissolution temperatures of phases in the entrapped fluids were measured by using the LINKAM MDS 600 and LINKAM THMSG 600 heating-freezing stages, which were calibrated with synthetic fluid inclusions at -56.6 °C (melting of CO_2), 0.0 °C (melting of H_2O), and 374.0 °C (critical density of H_2O). The instrument resolution of both stages is 0.1 °C, and the standard deviation in each measurement was ± 0.2 °C in the range of -50 to $+50$ °C, and increased towards higher temperatures, up to ± 0.5 °C at 400 °C. Fluid properties, i.e. (1) composition and (2) density, were calculated from the results of microthermometric investigations.

2.5. Calculation of fluid properties

The fluid properties were calculated with the software package FLUIDS (Bakker, 2003) and additional software from <http://fluids.unileoben.ac.at>. The salinity of H_2O -NaCl inclusions was calculated from dissolution temperatures of ice, T_m (ice), with the software AqSo WHS (Bakker, 2012; <http://fluids.unileoben.ac.at>). Inclusion density and molar volume were calculated from homogenization temperatures T_h (LV \rightarrow L). The properties of pure H_2O fluids were calculated with the equation of state from Haar et al. (1984) with the software Loner HGK (<http://fluids.unileoben.ac.at>). The software Loner AP and AqSo DH (<http://fluids.unileoben.ac.at>) were used for calculating density, molar volume, and homogenization temperatures for H_2O -NaCl fluid mixtures, with the equations from Anderko and Pitzer (1993), Driesner and Heinrich (2007), and Driesner (2007), respectively. The equation of state from Anderko and Pitzer (1993) provides the only possibility to calculate fugacities of H_2O in the binary H_2O -NaCl system. Table 3 shows calculated H_2O fugacities and molar volumes of the loaded fluid in the Au-capsules (Table 2) at experimental conditions, to illustrate fugacity gradients between synthesized fluid inclusions and re-equilibration conditions. A comparison between the equations of state is illustrated with e.g. GMR-004d, g in Table 3. In this experiment the pure H_2O fluid has a molar volume of 25.032 $cm^3 \cdot mol^{-1}$ according to Loner HGK. This value is reproduced by AqSo DH because the pure H_2O end-member fluid according to Haar et al. (1984) is part of that equation. The program Loner AP may also calculate pure H_2O end-member fluids of binary H_2O -NaCl mixtures, but has a higher uncertainty than Loner HGK. Nevertheless, the calculated molar volume is only 0.9% lower than that calculated with Loner HGK.

Table 2

Experimental conditions and fluid compositions of initial synthesis experiments (GMR) and corresponding re-equilibration experiments (R).

Experiment	Loaded fluid ^a		Hours ^b	p^c	Min–max ^d	T^e	Min–max ^f
	H ₂ O	NaCl					
GMR-004d, g	100	–	457.4	336.3 (0.46)	334.4–337.6	600.6 (0.41)	598.4–603.3
R-004d	80	20	462.5	337.4 (0.54)	327.2–338.4	599.9 (0.22)	599.4–600.7
R-004g	100	–	458.6	338.3 (0.26)	336.0–339.1	600.0 (0.25)	598.9–600.5
GMR-005a, b, c	80.2	19.8	458.6	336.9 (0.55)	335.3–338.5	600.7 (0.31)	598.8–601.1
R-005c	100	–	120.4	332.6 (0.30)	331.5–333.2	600.7 (0.50)	597.8–600.9
R-005a	100	–	459.8	336.1 (0.84)	334.8–338.0	600.7 (0.08)	598.9–600.8
R-005b	100	–	961.6	337.5 (1.57)	335.1–340.3	600.3 (0.31)	599.0–604.1
GMR-011a	90	10	462.4	337.4 (0.19)	336.6–338.0	599.7 (0.13)	598.2–600.3
R-011a	100	–	458.1	337.9 (0.39)	335.9–339.2	600.1 (0.24)	597.2–601.0
GMR-014a	83.7	16.3	454.3	337.4 (0.54)	332.5–338.2	600.4 (0.35)	597.2–601.1
R-014a	100	–	959.8	338.7 (0.13)	337.8–339.1	599.6 (0.24)	598.9–600.5

^a Composition in mass%.^b Experimentation time in hours.^c Average experimental pressure (in MPa) with standard deviation in brackets.^d Minimum and maximum pressures during experimental run (in MPa).^e Average experimental temperature (in °C) with standard deviation in brackets.^f Minimum and maximum temperatures during experimental run (in °C).

Loner HGK and AqSo DH are used to calculate theoretical homogenization temperatures of fluid inclusions from the experimental conditions of fluid entrapment (Table 3). Pure H₂O fluids trapped in the synthesis experiment GMR-004d and g should homogenize at 296.4 °C, corresponding to the calculated molar volume of 25.032 cm³·mol^{−1} at experimental conditions. The molar volume of α -quartz at experimental conditions is 23.152 cm³·mol^{−1} (Hosieni et al., 1985). At homogenization conditions, this molar volume is modified to 22.928 cm³·mol^{−1}, corresponding to a decrease of 0.9675% in total volume. Consequently, the molar volume of the fluid inclusions has to be corrected by −0.9675%. This correction results in higher densities, that corresponds to lower homogenization temperatures, i.e. 292.8 °C for the experiments GMR-004d and g (Table 3).

The theoretical homogenization temperatures of H₂O–NaCl inclusions (19.8 mass% NaCl) from synthesis experiments GMR-005a, b, and c are calculated at 329.6 °C. The quartz host contraction along the isochore towards homogenization conditions is about −0.7865 vol.%, which results in a minor correction of the molar volume to 23.546 cm³·mol^{−1} and lowering T_h by 5.3° to 324.3 °C (Table 3). The synthetic fluid inclusions with 10.0 mass% NaCl from synthesis experiment GMR-011a should have homogenization temperatures of 314.4 °C (corrected to 309.8 °C), whereas the synthesis experiment GMR-014a with 16.3 mass% NaCl aqueous fluid inclusions should reveal homogenization temperatures of 324.2 °C (corrected to 319.3 °C).

The expected dissolution temperatures of ice from inclusions of the initial synthesis are −16.5 °C, −12.4 °C, and −6.6 °C in the experiments GMR-005a–b–c, GMR-014a, and GMR-011a, respectively.

3. Experimental results

3.1. Blank re-equilibration experiments

The so called “blank” re-equilibration experiment was performed with the same fluid composition, i.e. pure H₂O, for both the original synthesis (GMR-004g) and the complementary re-equilibration (R-004g) at identical temperature and confining pressure, to check if the experimental setup and procedures are able to influence the properties of fluid inclusions.

Original pure H₂O inclusions display a variety of shapes after 457.4 h of experimentation, and are in general regularly shaped (Fig. 2). Most of the synthesized inclusions have a regular-equant shape, whereas some are regular-elongated. After re-equilibration in an identical H₂O fluid, only minor shape modifications occur towards more regular and equant shapes (Appendix).

Pure H₂O inclusions from GMR-004g homogenize at a mean T_h of 293.0 °C within the range of 290.3 to 295.2 °C (Table 4). The uniformity of this assemblage is illustrated in the histogram in Fig. 3a, and corresponds to the expected homogenization conditions according to the

Table 3

Calculated molar volumes (cm³·mol^{−1}) and H₂O fugacities (MPa) from experimental conditions of initial synthesis experiments (GMR) and corresponding re-equilibration experiments (R). The standard deviation (in brackets) is calculated from variations in experimental temperature and confining pressure, and does not include reported uncertainties of the equations of state. Software to calculate fluid properties is Loner HGK (Haar et al., 1984) for pure H₂O fluids, Loner AP (Anderko and Pitzer, 1993) for pure H₂O fluids and mixtures of H₂O–NaCl, and AqSo DH (Driesner, 2007). The software can be downloaded from the website <http://fluids.unileoben.ac.at> (Fluid Inclusion Laboratory Leoben, R. J. Bakker). The right column gives theoretical homogenization temperatures (T_h in °C) of fluid inclusions from the original synthesis experiments. T_h is obtained from molar volumes calculated with Driesner (2007) for NaCl–H₂O mixtures and Haar et al. (1984) for pure H₂O. Corrected T_h values according to contraction of quartz host (Hosieni et al., 1985) are given in brackets.

Experiment	Loner HGK		Loner AP		AqSo DH ^a	T_h
	V_m	$f(\text{H}_2\text{O})$	V_m	$f(\text{H}_2\text{O})$	V_m	
GMR-004d, g	25.032 (0.022)	175.76 (0.06)	24.811 (0.021)	169.94 (0.04)	25.032 (0.022)	296.4 (292.8)
R-004d	–	–	24.178 (0.011)	156.78 (0.37)	23.705 (0.011)	
R-004g	24.968 (0.013)	176.64 (0.03)	24.752 (0.012)	170.77 (0.01)	24.968 (0.013)	
GMR-005a, b, c	–	–	24.204 (0.014)	157.29 (0.13)	23.733 (0.013)	329.6 (324.3)
R-005c	25.128 (0.021)	173.58 (0.09)	24.895 (0.020)	167.86 (0.11)	25.128 (0.021)	
R-005a	25.040 (0.023)	175.69 (0.46)	24.818 (0.021)	169.88 (0.52)	25.040 (0.023)	
R-005b	24.995 (0.046)	176.32 (0.78)	24.777 (0.042)	170.47 (0.74)	24.995 (0.046)	
GMR-011a	–	–	24.417 (0.006)	164.15 (0.04)	24.165 (0.001)	314.4 (309.8)
R-011a	24.980 (0.016)	176.46 (0.10)	24.763 (0.015)	170.59 (0.09)	24.980 (0.016)	
GMR-014a	–	–	24.267 (0.015)	160.09 (0.10)	23.851 (0.015)	324.2 (319.3)
R-014a	24.948 (0.010)	176.67 (0.05)	24.733 (0.009)	170.78 (0.06)	24.948 (0.010)	

^a H₂O fugacities in H₂O–NaCl mixtures cannot be calculated with AqSo DH.

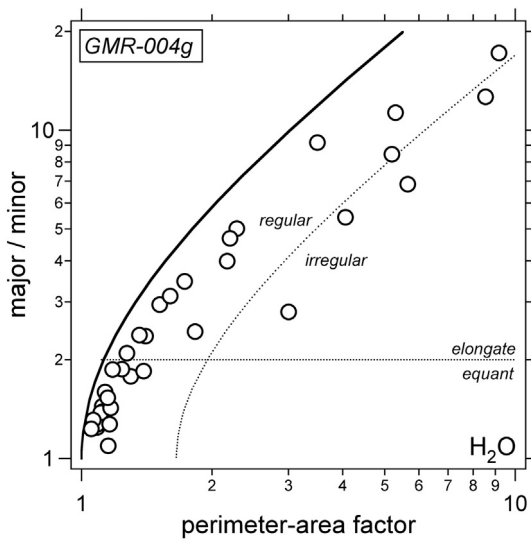


Fig. 2. Logarithmic fluid inclusions shape diagram according to Bakker and Diamond (2006) for experiment GMR-004g. The x-axis represents the perimeter-area factor: $p^2 / (4\pi a)$, where p is perimeter and a is area. The y-axis represents the ratio of length of the major and minor axis of the best-fit ellipse. The dashed lines divide the diagram in four regions according to the definition of regular, irregular, equant and elongate. The regular–irregular boundary is defined by stretching of equilateral triangle. The thick curved line is the limit of shape definitions. The axes are in logarithm-scale.

Table 4

Microthermometric properties of fluid inclusions after the initial synthesis experiments (GMR).

Experiment	n^a	T_h^b	st. dev. ^c	Range ^d	T_m^e	Range ^f
GMR-004d	97	292.5	0.8	289.5–295.6	0.0	0.0 to 0.0
GMR-004g	34	293.0	0.8	290.3–295.2	0.0	0.0 to 0.0
GMR-005c	67	328.3	2.5	321.5–332.1	–16.5	–
GMR-005a	94	329.7	1.5	324.4–332.8	–16.5	–16.3 to –16.6
GMR-005b	68	326.9	3.1	316.6–330.8	–16.9	–16.5 to –17.2
GMR-011a	95	313.9	0.8	311.8–318.8	–6.6	–6.1 to –6.7
GMR-014a	71	328.5	1.3	324.8–331.9	–12.4	–12.4 to –12.4

^a Number of measured fluid inclusions.

^b Mean T_h (homogenization temperature) in °C (LV → L).

^c Standard deviation T_h in °C.

^d Minimum and maximum T_h in °C.

^e Mean T_m (ice dissolution temperature) in °C (SLV → LV).

^f Minimum and maximum T_m in °C.

corrected isochore calculation (see Table 3). The distribution of T_h values illustrates that the fluid properties at experimental conditions are conserved within all fluid inclusions. After the blank re-equilibration experiment R-004g the mean T_h is only slightly modified to 292.3 °C, with a similar range from 289.6 to 295.3 °C (Table 5, Fig. 3b). Direct comparison of T_h of individual inclusions before and after re-equilibration (Fig. 3c) illustrates that multiple isochoric loading and unloading does not affect fluid properties such as density of the original synthesized inclusions.

3.2. Pure H₂O fluid inclusions re-equilibrated in 20 mass% NaCl aqueous solution

The fugacity gradient of H₂O between pure H₂O fluid inclusions and a 20 mass% NaCl pore fluid is about –13.2 MPa in re-equilibration experiment R-004d (Table 3). According to this gradient, it is expected that H₂O diffuses out of the fluid inclusions, whereas dissolved NaCl may diffuse into the fluid inclusions. These processes would modify the density and composition of the originally synthesized inclusions, which can be verified by measuring a modification in dissolution temperature of ice due to increased salinity, and an increase in homogenization temperature due to H₂O loss.

The shape and size variability of original synthesized pure H₂O fluid inclusions in the experiment GMR-004d (Fig. 4a, Appendix) are similar to those values illustrated for pure H₂O fluid inclusions from GMR-004g (Fig. 2). Significant shape modifications occur towards more regular and equant shapes after the re-equilibration experiments R-004d (Fig. 4b). Fig. 4c illustrates an example of an elongated fluid inclusion before and after re-equilibration.

The homogenization temperatures of pure H₂O inclusions from the synthesis experiment GMR-004d reveal a normal distribution (Fig. 5a), similar to the previously mentioned experiment GMR-004g (c.f. Fig. 3a). The mean T_h of GMR-004d is 292.5 °C (Table 4) with a standard deviation of 0.8 °C. T_h varies between 289.5 and 295.6 °C. These temperatures correspond to the expected values according to the isochore correction from experimental conditions to homogenization conditions that are given in Table 3. Homogenization temperatures are modified to higher values compared to the original synthesis (Fig. 5b, c), which correspond to lower densities and the loss of H₂O. The mean T_h in R-004d increases to 294.4 °C, with a similar standard deviation of 0.8 °C (Table 4). This modification is consistent with the expected H₂O diffusion out of fluid inclusions according to the H₂O fugacity gradient (Table 3).

A modification of T_m (ice) in fluid inclusions is not observed after re-equilibration with a 20 mass% NaCl aqueous solution pore fluid at the same temperature and confining pressure conditions. The diffusion of

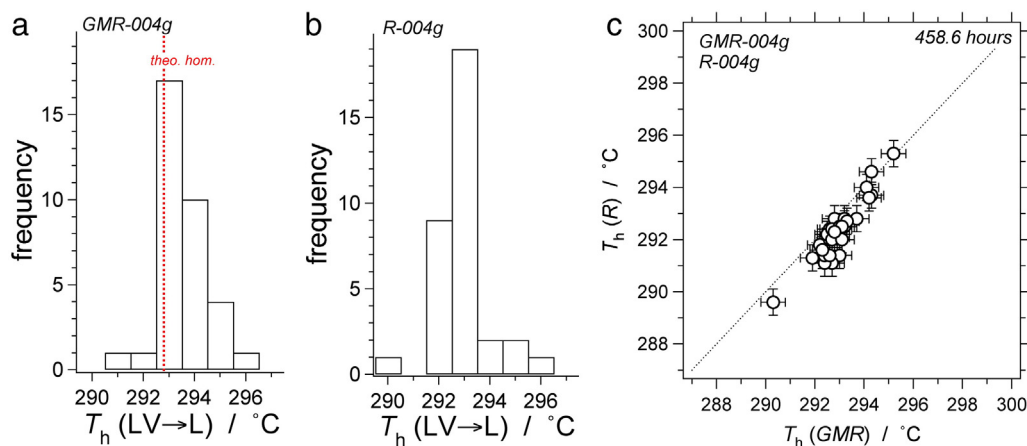


Fig. 3. Histograms of T_h (pure H₂O fluid inclusion) of the synthesis experiments GMR-004g (a) and corresponding “blank” re-equilibration experiment R-004g in pure H₂O (b). Direct comparison of T_h values of individual inclusions from the synthesis and re-equilibration is illustrated in (c). The dashed diagonal line in (c) illustrates conditions of no modifications.

Table 5

Microthermometric properties of fluid inclusions after the re-equilibration experiments (R).

Experiment	n^a	T_h^b	st. dev. ^c	Range ^d	T_m^e	Range ^f
R-004d	68	294.4	0.8	292.3–297.6	0.0	0.0 to –0.1
R-004g	34	292.3	1.1	289.6–295.3	0.0	–
R-005c	67	326.5	3.0	319.6–332.4	–17.1	–14.5 to –18.1
R-005a	87	333.1	1.8	328.1–336.4	–18.9	–17.2 to –20.2
R-005b	66	327.3	3.6	327.6–342.1	–21.0	–15.6 to –22.2
R-011a	95	312.4	0.6	310.7–314.5	–7.2	–6.8 to –7.5
R-014a	67	335.3	1.3	331.8–338.4	–16.0	–14.0 to –16.5

^a Number of measured fluid inclusions.

^b Mean T_h (homogenization temperature) in °C (LV → L).

^c Standard deviation T_h in °C.

^d Minimum and maximum T_h in °C.

^e Mean T_m (ice dissolution temperature) in °C (SLV → LV).

^f Minimum and maximum T_m in °C.

NaCl or a 20 mass% NaCl aqueous solution towards fluid inclusions was not demonstrated in our experimental setup, and is, therefore, assumed to be highly inefficient or virtually impossible in geological processes.

3.3. Aqueous fluid inclusions with 10 mass% NaCl re-equilibrated in pure H₂O

The fugacity gradient of H₂O between 10 mass% NaCl aqueous fluid inclusions and a pure H₂O pore fluid is about +6.4 MPa in the re-equilibration experiment R-011a (Table 3). H₂O is expected to diffuse

into fluid inclusions according to this gradient, resulting in higher densities and lower salinities that correspond to lower T_h and higher T_m values.

Fluid inclusions with 10 mass% NaCl aqueous solution, that are originally synthesized in GMR-011a have regular shapes, approximately negative-crystal shapes, and vary from equant to elongated (Fig. 6a, Appendix). After 458.1 h of re-equilibration at similar conditions in pure H₂O, the inclusions do not reveal significant modifications in shape parameters.

The inclusions from GMR-011a homogenize at a mean T_h of 313.9 °C (Table 4), which does not correspond to the predicted homogenization conditions according to the corrected isochore calculation at 309.8 °C (Table 2). Nevertheless, the assemblage has uniform properties and reveals a normal distribution with a relative large standard deviation (Fig. 6b). The spread in T_h is larger than the values recorded for pure H₂O fluid inclusions from GMR-004d and g. After re-equilibration (R-011a), T_h 's are modified to lower values (Fig. 6c) as expected from H₂O-diffusion into inclusions. The mean T_h after re-equilibration is 312.4 °C within a range of 310.7 to 314.5 °C (Table 4). Individual T_h 's are lowered maximally by 6°.

T_m (ice) of fluid inclusions from GMR-011a varies between –6.1 and –6.7 °C (Table 4) with a mean value at –6.6 °C, which corresponds to the expected T_m according to a 10 mass% NaCl aqueous solution. This temperature is modified to a mean value of –7.2 °C and a range of –6.8 to –7.5 °C (Fig. 6c, Table 5) after 458.1 h of re-equilibration. This modification does not correspond to the expected dilution of inclusions due to H₂O in-diffusion (i.e. gain of H₂O), but indicates a preferential loss of H₂O.

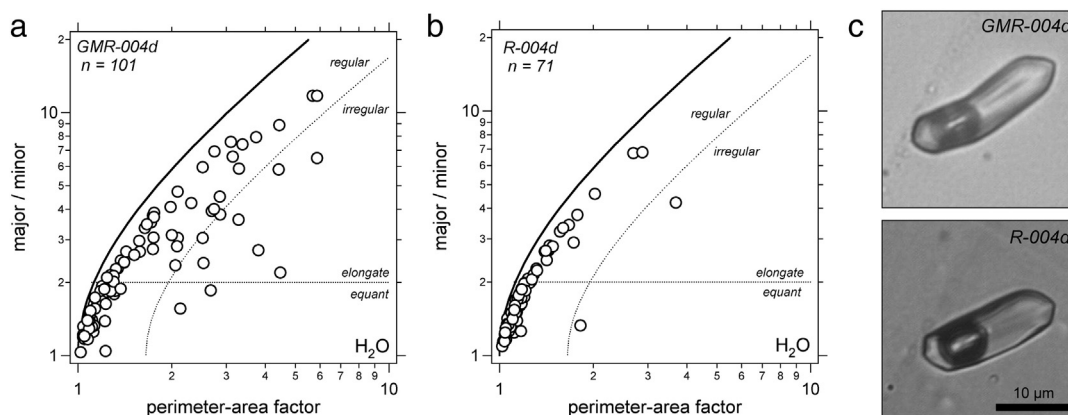


Fig. 4. Logarithmic fluid inclusions shape diagram for the synthesis experiments GMR-004d (a) and corresponding re-equilibration experiment R-004d (b). Photomicrographs of fluid inclusions before and after re-equilibration are illustrated for GMR-004d and R-004d in (c).

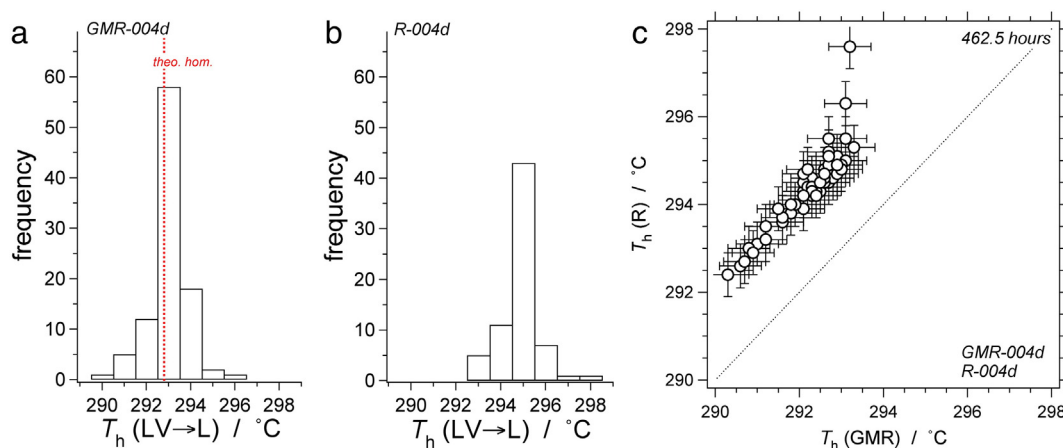


Fig. 5. Histograms of T_h (pure H₂O fluid inclusions) of the synthesis experiments GMR-004d (a) and corresponding re-equilibration experiment R-004d in a 20 mass% NaCl solution (b). Direct comparison of T_h values of individual inclusions from the synthesis and re-equilibration is illustrated in (c). The dashed diagonal line in (c) illustrates conditions of no modifications.

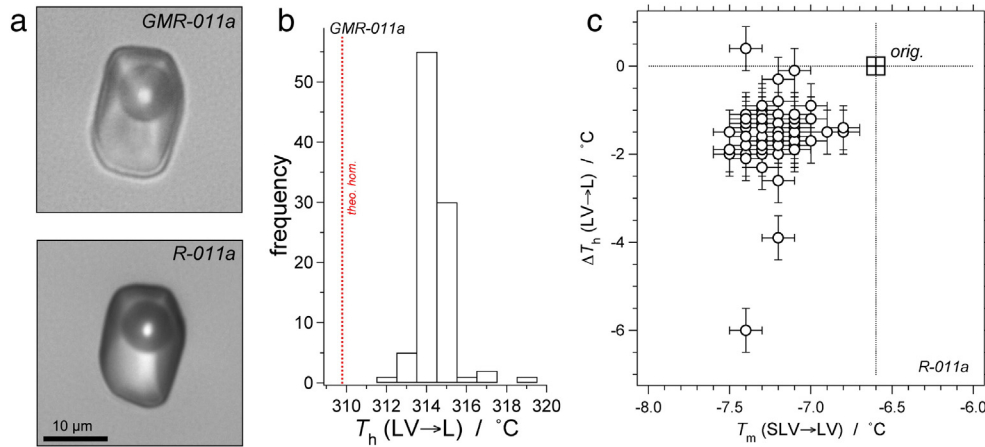


Fig. 6. (a) Photomicrograph of a fluid inclusion (10 mass% NaCl solution) from synthesis experiment GMR-011a and corresponding re-equilibration experiment R-011a in pure H₂O. (b) Histogram of T_h of the synthesis experiment GMR-011a. The vertical dashed red line indicates the theoretical T_h value according to the experimental conditions. (c) The change in T_h versus T_m illustrates the shift in fluid properties of individual fluid inclusions. (For interpretation of the references to color in this figure legend, the reader is referred to the web version of this article.)

3.4. Aqueous fluid inclusions with 16.3 mass% NaCl re-equilibrated in pure H₂O

The fugacity gradient of H₂O between 16.3 mass% NaCl aqueous fluid inclusions and a pure H₂O pore fluid is about +10.69 MPa in the re-equilibration experiment R-014a (Table 3). This gradient is larger than in the previously described re-equilibration experiment R-011a, and, therefore, H₂O diffusion into the fluid inclusions is expected to be more efficient, resulting in lower T_h and higher T_m .

Similar to all the other experiments with H₂O–NaCl solutions, the synthesized fluid inclusions (GMR-014a) have more regular shapes than pure H₂O inclusions and approximate negative-crystal shapes (Fig. 7a, Appendix). Inclusion shapes vary from equant to elongated. After re-equilibration of 959.8 h (R-014a), the shape parameters of inclusions are not significantly modified.

The mean T_h after the original experiment GMR-014a is 328.5 °C, within a range of 324.8 to 331.9 °C (Table 4). The distribution of T_h values (Fig. 7b) is slightly asymmetric with a small tail towards lower T_h values. However, the mean T_h does not reflect the experimental conditions that result in an isochore corrected value of 319.3 °C (Table 3). The observed T_h 's are even exceeding the uncorrected value of 324.2 °C. After a long-term (959.8 h) re-equilibration in pure H₂O at similar temperature and pressure conditions (R-014a), T_h 's are modified to significantly higher values, in contrast to the previously described re-equilibration experiment R-011a, with a mean T_h of 335.3 °C in the

range 331.8 to 338.4 °C (Fig. 7c, Table 5). This modification may be caused by significant preferential H₂O loss, and is much stronger than the opposite H₂O-gain in experiment R-011a.

All the original synthesized fluid inclusions have T_m (ice) of −12.4 °C, corresponding to the experimental setup with a 16.3 mass% NaCl aqueous solution. T_m (ice) decreases significantly in individual inclusions after 959.8 h of re-equilibration (R-014a), resulting in a mean T_m of −16.0 °C within a range of −14.0 to −16.5 °C (Fig. 7c, Table 5). This modification is also larger than in the previously described re-equilibration experiment R-011a. Moreover, these modifications are apparently consistent with the increase in T_h , due to preferential loss of H₂O. However, it is in contrast to the expected modifications according to the imposed H₂O fugacity gradient.

3.5. Aqueous fluid inclusions with 19.8 mass% NaCl re-equilibrated in pure H₂O

Synthesized 19.8 mass% NaCl aqueous inclusions (GMR-005a, b, and c) are re-equilibrated in pure H₂O at various experimental run-times: for 120.4 h (R-005c), for 459.8 h (R-005a), and for 961.6 h (R-005b) (Table 2). It is expected that H₂O will diffuse into fluid inclusions according to fugacity gradients of +10.57 to +13.18 MPa at experimental conditions (Table 3). The expected H₂O enrichment should result in lower salinities (i.e. higher T_m), and higher density (i.e. lower T_h). Modifications in fluid inclusion salinity and density should progress

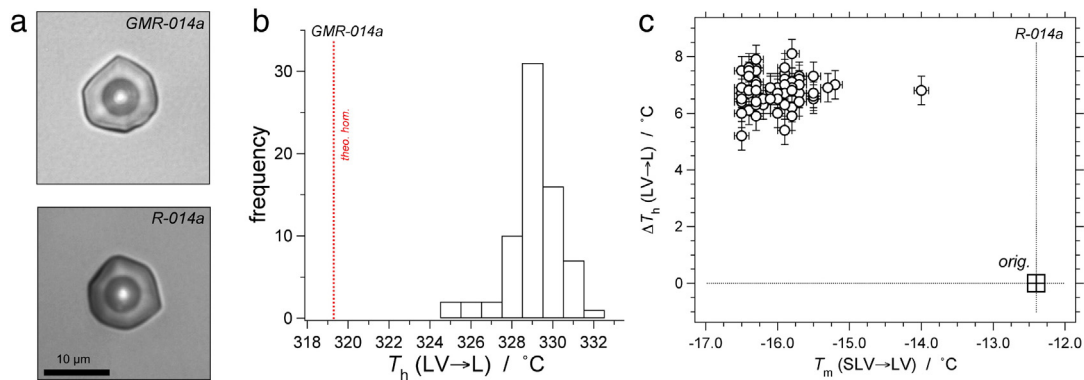


Fig. 7. (a) Photomicrograph of a fluid inclusion (16.3 mass% NaCl) from synthesis experiment GMR-014a and corresponding re-equilibration experiment R-014a in pure H₂O. (b) Histogram of T_h of the synthesis experiment GMR-014a. The vertical dashed red line indicates the theoretical T_h value according to the experimental conditions. (c) The change in T_h versus T_m illustrates the shift in fluid properties of individual fluid inclusions. (For interpretation of the references to color in this figure legend, the reader is referred to the web version of this article.)

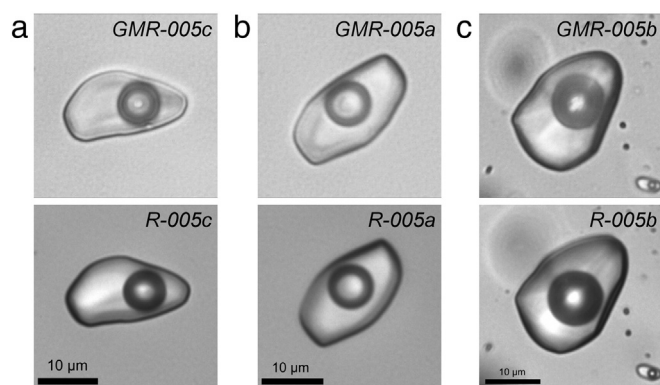


Fig. 8. Photomicrographs of identical fluid inclusions (original composition 19.8 mass% NaCl) before and after re-equilibration of the experiments (a) *GMR-005c* and *R-005c*, 120.4 h; (b) *GMR-005a* and *R-005a*, 459.8 h; (c) *GMR-005b* and *R-005b*, 961.6 h.

with increasing re-equilibration time according to the principles of diffusion.

Most fluid inclusions that have been synthesized with 19.8 mass% NaCl in the experiments *GMR-005c*, *a*, and *b* showed regular and equant shapes and do not change significantly their morphology after re-equilibration (Fig. 8a, b, and c, respectively) (Appendix). The inclusion morphology approaches negative crystal shapes, and the perfection of this shape does not provide a driving force for shape modifications during re-equilibration.

The mean T_h after the synthesis *GMR-005a*, *GMR-005b*, and *GMR-005c* is 329.7, 326.9, and 328.3 °C, respectively (Table 4). The spread in T_h values is relatively large and the distribution of T_h reveals an asymmetric pattern with a tail towards lower T_h in histograms (Fig. 9). Furthermore, the mean values do not correspond to the theoretical value at 324.3 °C according to the isochore correction (Table 3). The mean T_h is modified to 326.5 °C after 120.4 h (*R-005c*, Table 5, Fig. 10) with a slightly larger spread, which corresponds to a minor increase in density. This increase can only be obtained by adding H₂O to the inclusions by diffusional processes or by loss of total inclusion volume at constant temperature and pressures. In contrast, the trend in modification of T_h illustrates higher values for longer re-equilibration experiments (Fig. 10, 459.8 and 961.6 h). Re-equilibration experiment *R-005a* (459.8 h) reveals a mean T_h of 333.1 °C with a variation of 328.1 to 336.4 °C (Table 5), whereas those values increased to an average of 337.3 °C and a variation of 327.6 to 342.1 °C after 961.6 h of re-equilibration (*R-005b*) (Table 5). This increase in T_h corresponds to a decrease in fluid inclusion density by definition, consequently, inclusions in the

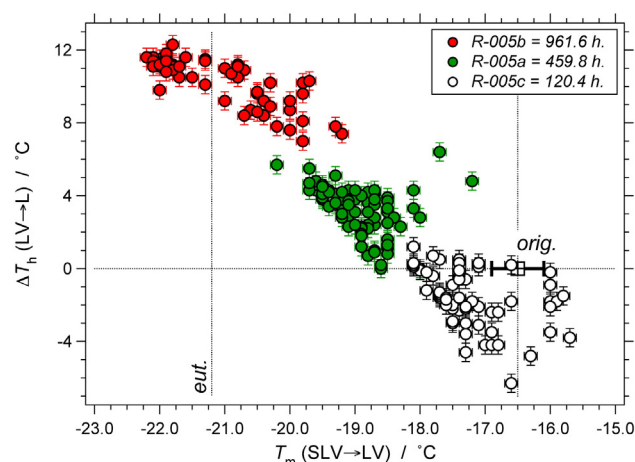


Fig. 10. Diagram of the change in T_h versus T_m of individual fluid inclusions (original composition 19.8 mass% NaCl) to illustrate the shift in fluid properties after the re-equilibration experiments *R-005c*, *R-005a*, and *R-005b* in pure H₂O.

long-term experiments must have lost fluid components according to diffusional processes, but against the imposed H₂O fugacity gradient.

The dissolution temperatures of ice in the original synthesized inclusions from the experiments *GMR-005a*, *b*, and *c* have a mean value of −16.5 to −16.9 °C, and reveal a spread between −16.3 and −17.2 °C (Table 4). This spread illustrates that a minor variation in salinity occurs in single fluid inclusion assemblages that are synthesized from a homogeneous pore fluid. After 120.4 h of re-equilibration (*R-005c*) at a similar temperature and confining pressure, the mean T_m (ice) is modified to −17.1 °C, which is a decrease of 0.6° (Fig. 10, Table 5). The mean temperature corresponds to a salinity of 20.3 mass% NaCl. After 459.8 h of re-equilibration (*R-005a*) fluid inclusion compositions are further modified to higher salinities (21.6 mass% NaCl) as reflected by a mean T_m (ice) of −18.9 °C (Table 5). T_m (ice) is further modified in the long-term re-equilibration experiment (961.6 h, *R-005b*) to a mean value of −21.0 °C, corresponding to a salinity of 23.3 mass% NaCl (Table 5). A remarkable result is that part of the T_m (ice) measurements is at temperatures below the eutectic temperature of the binary H₂O–NaCl system (Fig. 10).

In microthermometric heating–freezing experiments, the original synthesized fluid inclusions reveal low temperature behavior according to the binary H₂O–NaCl system (c.f. Bakker, 2004), i.e. nucleation of a glass occurs at about −67 °C during a freezing experiment (Fig. 11a); recrystallisation during heating to a mixture of ice and hydrohalite is clearly visible at −22 °C, followed by the phase transition at the eutectic

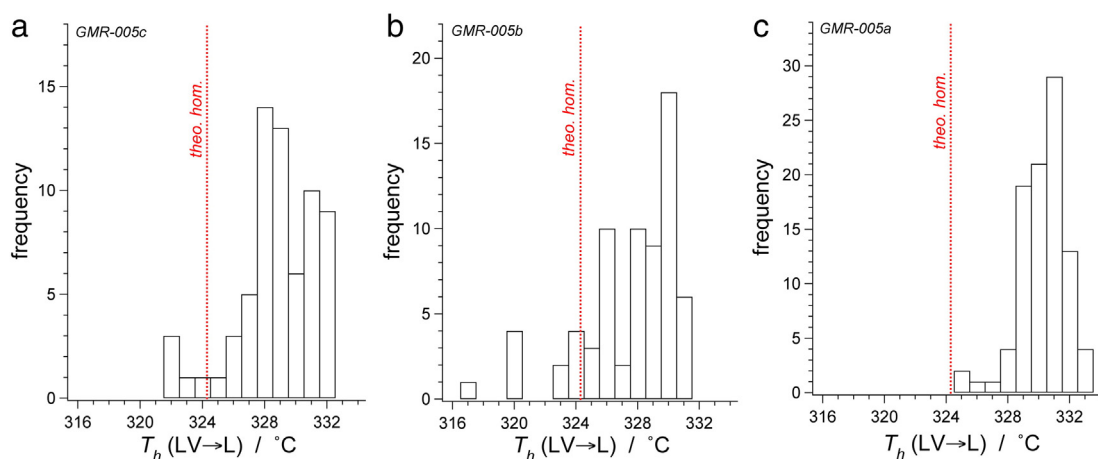


Fig. 9. Histograms of T_h (19.8 mass% NaCl fluid inclusions) from the synthesis experiments *GMR-005c* (a), *GMR-005b* (b), and *GMR-005a* (c). The vertical dashed red line indicates the theoretical T_h value according to the experimental conditions. (For interpretation of the references to color in this figure legend, the reader is referred to the web version of this article.)

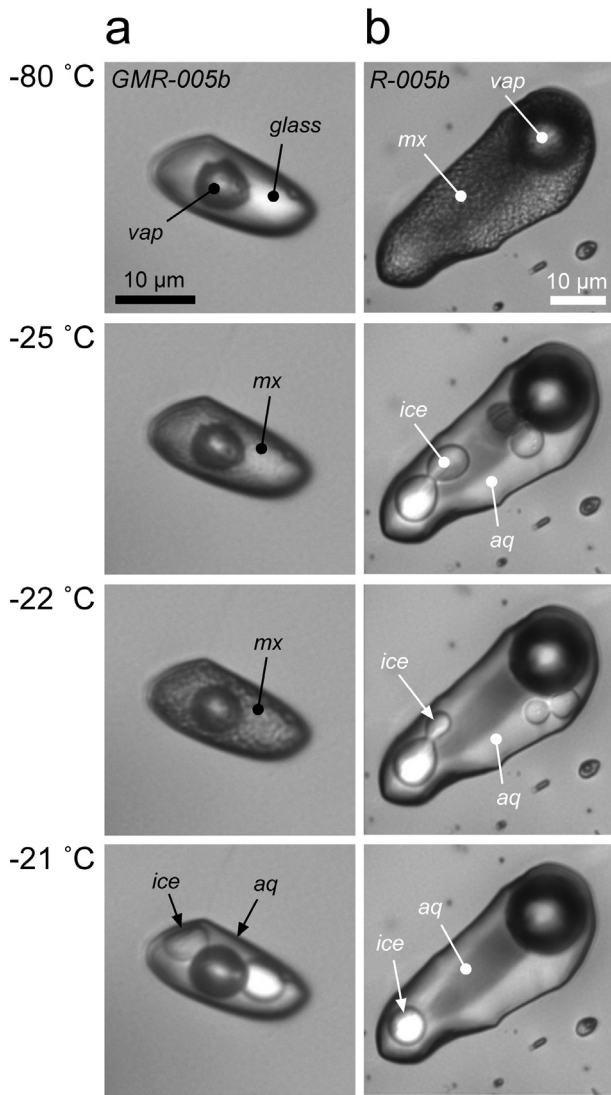


Fig. 11. Photomicrographs of fluid inclusions from the original synthesis experiment GMR-005b (a) and corresponding re-equilibration experiment R-005b (b) of a freezing and heating experiment illustrating the phase assemblages within individual inclusions at $-80\text{ }^{\circ}\text{C}$, $-25\text{ }^{\circ}\text{C}$, $-22\text{ }^{\circ}\text{C}$ and $-21\text{ }^{\circ}\text{C}$. vap = vapor, mx = micro-crystalline mixture of ice and hydrohalite, aq = aqueous liquid solution.

temperature ($-21.2\text{ }^{\circ}\text{C}$) to a brine and ice in the presence of a vapor bubble. The ice finally dissolves at $-16.5\text{ }^{\circ}\text{C}$ in this example. The re-equilibrated inclusions from R-005b reveal a different microthermometrical behavior at low temperatures (Fig. 11b), i.e. nucleation during a cooling experiment already produces a microcrystalline mixture of ice and hydrohalite at $-67\text{ }^{\circ}\text{C}$ (the so-called “orange-skin” texture); during a heating experiment, the first liquid phase is already visible at $-28\text{ }^{\circ}\text{C}$ in the presence of ice, hydrohalite and a vapor bubble; hydrohalite finally dissolves at $-25.8\text{ }^{\circ}\text{C}$, whereas the final ice dissolution temperature is $-19.8\text{ }^{\circ}\text{C}$. Comparison of hydrohalite dissolution temperatures between original inclusions and re-equilibrated inclusions is illustrated in Fig. 12. The relatively low temperatures in re-equilibrated inclusions suggest the presence of other dissolved species in addition to NaCl.

Comparison of modifications in T_h and T_m (ice) of individual fluid inclusions (Fig. 10) demonstrates that diffusional H_2O loss at experimental conditions of about $600\text{ }^{\circ}\text{C}$ and 336 MPa is the main process that affect fluid inclusions in relative long re-equilibration experiments (up to 961.6 h). It must be noted that this process is not consistent with the theoretically predicted modifications according to the applied

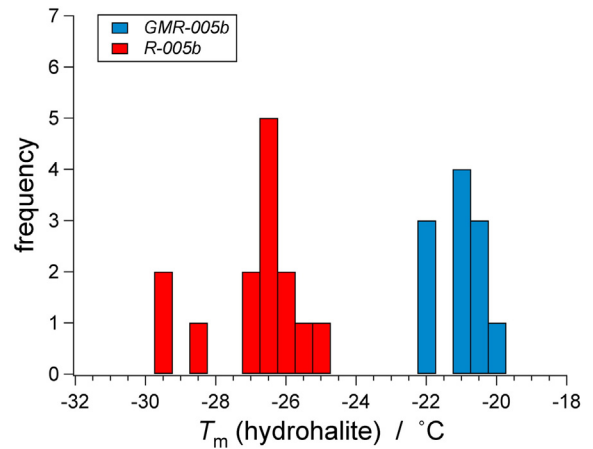


Fig. 12. Histograms of T_m (hydrohalite) from the original synthesis experiment GMR-005b and corresponding re-equilibration experiment R-005b.

gradient in H_2O fugacity (see Table 2). Furthermore, the fluid composition in inclusions has evolved from a binary H_2O –NaCl system to a multi-component system after re-equilibration. The identity of additional components is not determined in the present study, but could be analyzed by LA-ICP-MS (e.g. Pettke et al., 2012) in future research.

4. Discussion

4.1. Inconsistent synthesis?

The homogenization temperatures of H_2O –NaCl fluid inclusions in the original synthesis experiments GMR-005a, b, c, GMR-011a, and GMR-014a do not correspond to the experimental conditions (Figs. 6, 7, and 9). This discrepancy seems to be a common phenomenon in previous experimental fluid inclusion studies, but remained unnoticed. For example, fluid inclusions with 20.8 mass% NaCl (4.5 M) were synthesized at $611\text{ }^{\circ}\text{C}$ and 300 MPa by Zhang and Frantz (1987). These inclusions have a molar volume of $24.502\text{ cm}^3\cdot\text{mol}^{-1}$ according to Driesner (2007), which is corrected to $24.269\text{ cm}^3\cdot\text{mol}^{-1}$ at homogenization conditions according to quartz host volumetric properties (Hosieni et al., 1985). This corrected molar volume corresponds to a $T_h = 344.4\text{ }^{\circ}\text{C}$, which is significantly lower than the measured T_h of $353.4\text{ }^{\circ}\text{C}$ (Zhang and Frantz, 1987), and similar to the discrepancy observed in our study. In contrast, such discrepancies do not occur in pure H_2O fluid inclusions, as illustrated by the results of synthesis experiments GMR-004d and g (see also Figs. 3 and 5), where the experimental conditions define exactly the homogenization temperatures.

The most obvious explanation for these discrepancies is that the uncertainty in V_m calculations of binary H_2O –NaCl mixtures according to Driesner (2007) causes apparent differences between trapping conditions and homogenization conditions. Driesner (2007) illustrated an average 0.9% uncertainty in calculated V_m compared to experimental data at high temperatures and pressures, and 0.05 to 0.5% at homogenization conditions. The uncertainties at experimental trapping conditions of the synthesized fluid inclusions would result in approximately 6° of uncertainty in homogenization temperatures. The average uncertainty in density calculation of pure H_2O according to Haar et al. (1984) is about 0.5% at the trapping conditions, and about 0.1% at homogenization conditions. The corresponding uncertainty in homogenization temperatures would be 1.8° . These uncertainty considerations do not explain the large differences between calculated and measured homogenization temperatures of H_2O –NaCl fluid inclusions in our experiments (e.g. Fig. 7), or the relatively large spread in T_h values after the original synthesis of H_2O –NaCl fluid inclusions (e.g. Fig. 9), whereas H_2O fluid inclusions reveal a perfect fit between calculated V_m values at trapping conditions and homogenization conditions.

Deviating molar volumes of H₂O–NaCl-bearing fluid inclusions that are synthesized at a constant temperature and confining pressure can only be obtained by modification of total volume of the host crystal immediately after fluid entrapment. A logical conclusion would be to assume that the newly grown quartz in the cracks has different properties than the original quartz core, and that hysteresis, ripening or an irreversible thermodynamic change is affecting the volume of the newly formed fluid inclusions. Volume modifications must have occurred already during the synthesis resulting in small pressure differences between the pore fluid (and host quartz) and fluid inclusions, which are not sufficient to initiate textural modifications. The calculated volume correction is about +4% of the total volume.

4.2. Diffusion processes and volume modifications in R-004d

Diffusion of H₂O through quartz from and to fluid inclusions at constant temperature and confining pressure was experimentally proven by e.g. Doppler et al. (2013). Diffusion of H₂O is expected in the re-equilibration experiment R-004d due to the H₂O fugacity gradient between original synthesized inclusions and the surrounding pore fluid (Table 2). The maximum modification of these fluid inclusions can be calculated with the software *ReqDif* according to the diffusion model from Bakker (2009). After a hypothetical diffusion in experiment R-004d, upon reaching equal H₂O fugacities within the fluid inclusion and the pore fluid, the molar volume will be modified by +2.1%, i.e. a slightly lower density. This corresponds to a decrease in $x(\text{H}_2\text{O})$ by 2.1%, if the total volume of the fluid inclusion remains constant. This loss results in a modification of T_h to about 300.3 °C (c.f. 292.5 °C in GMR-004d, Table 4), taking into account the isochore correction according to the modifications in the quartz molar volume. However, the average shift in T_h observed in experiment R-004d is only about +2° (294.4 °C, Table 5). The H₂O fluid properties in the fluid inclusion assemblage in R-004d illustrate that equality in fugacity is not reached after 19 days of experimentation.

Diffusion is a time-dependent process, therefore, larger modifications are expected due to longer experimental runtimes. Doppler et al. (2013) illustrated the variability in modification of individual fluid inclusions in a single quartz grain due to time, temperature, inclusion size, and distance of inclusions to the quartz rim. After re-equilibration experiment R-004d, the fluid inclusion assemblage illustrates a homogeneous modification, independent from the original variability in T_h (Fig. 5), which may indicate that none of the abovementioned factors (e.g. distance to quartz rim) play a role.

The change in total volume of individual fluid inclusions can be a second process that affects the fluid properties. Higher fluid densities can be obtained if the total fluid inclusion volume becomes smaller. This modification corresponds to a decrease in T_h . Changes in total volume are mainly caused by pressure differences between inclusions and pore fluids. For example, an internal overpressure may cause the spontaneous formation of microcracks around fluid inclusions that increase the total volume. Fluids may be lost completely if these microcracks reach the surface of the quartz grain (decrepitation). In contrast, a fluid underpressure may cause the “collapse” of fluid inclusions (e.g. Sterner and Bodnar, 1989). Variability in quartz solubility around an under-pressurized fluid inclusion was suggested by Bakker (2009) to cause the irregular shapes of these inclusions as illustrated in previous studies. The responsible process combines the movement of SiO₂ molecules from the surrounding quartz into the inclusions (c.f. silicon self-diffusion, Chermiak, 2003) simultaneously with the movement of H₂O away from the inclusions (Fig. 10 in Bakker, 2009). The experimental setup of R-004d defines a constant temperature and pressure in the re-equilibration experiment. However, diffusion of H₂O out of the inclusions causes a decrease in internal pressure, down to about 311.4 to 314.8 MPa, which is an underpressure of about –23.5 MPa (calculated with software *ReqDif*, Bakker, 2009). Therefore, diffusion triggered by a

H₂O fugacity gradient at constant temperature and confining pressure results in a pressure gradient.

In conclusion, preferential diffusion of H₂O out of fluid inclusions according to fugacity gradients is the initial process that affects fluid inclusions in our re-equilibration experiments. This process causes an increase in T_h . Subsequently, the produced internal under-pressure results in a total volume decrease in order to reduce the pressure gradient, resulting in lower T_h values. The net modification of T_h is about +2 °C. The total volume decrease is difficult to detect in two-dimensional images because only minor modifications are involved. However, comparison of total area of individual fluid inclusions before and after re-equilibration illustrates a minor average decrease (Appendix).

4.3. Theoretical salinity and density modifications of H₂O–NaCl bearing fluid inclusions

The previously mentioned processes can be applied to original H₂O–NaCl bearing fluid inclusions to model the coupled modifications in salinity and molar volume. Preferential loss and gain of H₂O have specific effects on both salinity and molar volume of fluid inclusions with a constant total volume.

A hypothetical fluid inclusion with the same fluid properties as those observed in synthesis experiment GMR-005a is used to illustrate systematic modifications in salinity and density due to preferential H₂O loss and gain (Table 6). The original salinity is 19.8 mass% NaCl, and the molar volume is 23.733 cm³·mol^{–1} (see Table 2), corresponding to a T_m (ice) = –16.5 °C and T_h (LV → L) = 329.7 °C. Table 6 illustrates that T_h is a very sensitive indicator of minor amounts of H₂O loss: 1% loss of amount of substance already results in a 6.4 °C increase in T_h , whereas the change in salinity only results in minor modifications of T_m (ice). The observed modification of T_m (ice) to –18.8 °C after the re-equilibration experiment (c.f. Table 4) corresponds to 10% preferential loss of the amount H₂O. Consequently, the molar volume is modified to 26.164 cm³·mol^{–1}, which corresponds to T_h (LV → L) = 393.6 °C. These theoretical values are inconsistent with the observed T_h of about 333.1 °C (Table 4). A decrease in total fluid inclusion volume is the only process that may explain this discrepancy, since the mobility of NaCl is excluded according to the results of the re-equilibration experiment R-004d.

4.4. Mobility of H₂O and volume modifications in R-005a, b, and c

Re-equilibration experiments R-005a, b, and c illustrate modifications of 19.8 mass% NaCl aqueous inclusions at variable experimental

Table 6

Theoretical modifications in salinity, $x(\text{NaCl})$ and mass% NaCl, molar volume (V_m) and microthermometric properties as a consequence of preferential H₂O loss (in amount-of-substance fraction, also known as “mole %”) from a H₂O–NaCl bearing fluid inclusion.

Pref. water loss (mole %)	$x(\text{NaCl})$	Mass% NaCl	V_m cm ³ ·mol ^{–1}	T_m (ice) °C	T_h^a °C
0	0.07072	19.80	23.733	–16.5	329.7
1	0.07138	19.96	23.956	–16.7	336.1
2	0.07206	20.12	24.182	–16.9	342.5
3	0.07275	20.29	24.414	–17.1	348.9
4	0.07345	20.46	24.649	–17.3	355.2
5	0.07417	20.63	24.890	–17.6	361.5
6	0.07490	20.80	25.134	–17.8	367.8
7	0.07564	20.98	25.384	–18.0	374.2
8	0.07640	21.16	25.639	–18.3	380.4
9	0.07718	21.34	25.899	–18.5	386.8
10	0.07800	21.53	26.164	–18.8	393.6
11	0.07877	21.72	26.435	–19.1	400.2
12	0.07960	21.91	26.712	–19.3	406.9
13	0.08044	22.10	26.994	–19.6	413.7
14	0.08130	22.30	27.282	–19.9	420.7
15	0.08218	22.51	27.577	–20.2	427.9

^a Calculated with software *AqSo DH*.

run-times. A H_2O fugacity gradient of 10.57 to 13.18 MPa (Table 3) is present in each of these experiments at the start of re-equilibration. In addition, fluid inclusion assemblages in each re-equilibration experiment have variable pressure gradients due to the unexpected results from the synthesis experiment (e.g. 0 to –20 MPa underpressure in R-005a).

The observed modification in salinity (Fig. 10) corresponds to preferential loss of H_2O according to diffusion processes. The relative short-run experiment R-005c (120.4 h) reveals an average 3.0% preferential loss of the amount of H_2O , the intermediate-run R-005a (459.9 h) 10.3%, and the long-run R-005b (961.9 h) 17.5%. However, these modifications are inconsistent with the applied H_2O fugacity gradients that must result in the inward diffusion of H_2O , i.e. the preferential gain of H_2O . Furthermore, the corresponding modifications in T_h are not consistent with the abovementioned average preferential loss of H_2O (c.f. Table 6). The pressure gradient between inclusions and pore fluid may thus trigger total volume modifications. Inclusions in all re-equilibration experiments have underpressure, which must result in a decrease in total volume.

The precisely calculated amounts of H_2O loss from salinity modifications can be combined with precise calculations of total volume loss in order to obtain the observed densities. The relative short-run experiment R-005c (120.4 h) reveals an average loss of 3.4 vol.%, the intermediate-run R-005a (459.9 h) 9.7 vol.%, and the long-run R-005b (961.9 h) 16.2 vol.%, in order to obtain the observed molar volumes (Fig. 13). In contrast to apparent inconsistent modifications in T_h 's and T_m 's, the calculated values in preferential H_2O loss and total volume loss are illustrating a perfect linear trend according to experimental run times (Fig. 13).

The molar volumes of the fluid and the quartz are similar at experimental conditions: $23.171 \text{ cm}^3 \cdot \text{mol}^{-1}$ for quartz and $23.733 \text{ cm}^3 \cdot \text{mol}^{-1}$ for the fluid. Replacement of one mole fluid from the inclusion with one mole quartz would result in the coupled modifications in fluid density and total volume. In other words, each mole of H_2O that diffuses into the surrounding quartz is replaced by 1 mol of quartz that precipitates in the former inclusion volume, thus reducing its total volume. This process must be triggered by pressure gradients, whereas a simultaneously present fugacity gradient only takes into account minor modifications, which cannot be traced. Modifications in total volume of individual inclusions can be obtained from area analyses in two-

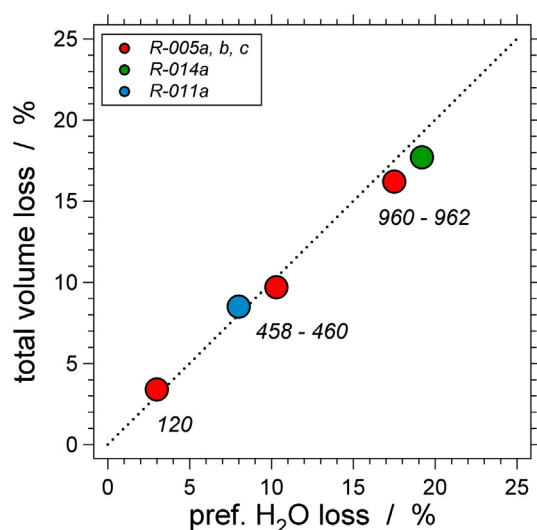


Fig. 13. Diagram of calculated preferential H_2O loss (in amount of substance %) versus total volume loss (in %) of the re-equilibration experiments R-005a, b, and c, R-011a, and R-014a. The numbers within the diagram illustrate run times (in hours) of the individual re-equilibration experiments. The dashed diagonal line indicates equal percentages in H_2O loss and total volume loss. The size of the symbols illustrates the variability of the fluid inclusion assemblage.

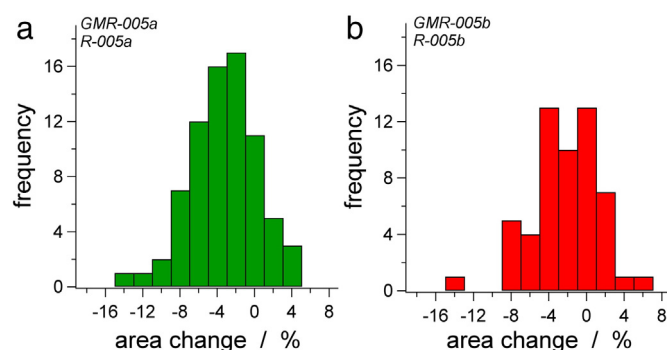


Fig. 14. Histograms with relative modifications in area (in %) of two-dimensional images of fluid inclusions after re-equilibration experiments R-005a (a) and R-005b (b).

dimensional images before and after re-equilibration (Fig. 14). The first impression from comparing images of individual inclusions is that total volume modifications are not significant (cf. Fig. 8). However, careful tracking the outline of inclusions in image analyzing software (ImageJ, <http://imagej.nih.gov/ij/>) reveals a significant decrease in total area (Fig. 14).

4.5. Size dependent modifications

The re-equilibrated fluid inclusion assemblages contain a large variety of fluid inclusion sizes (Appendix). For example in experiment R-005a, smaller inclusions reveal a large variety in T_h modifications, whereas larger inclusions are restricted to a relative small range (Fig. 15a). The trend in microthermometrical modifications according to inclusion size was illustrated by Doppler et al. (2013) using the H_2O diffusion model of Bakker (2009): larger inclusions reveal less modifications than small inclusions. This trend is approximately illustrated in Fig. 15a by the highest values of the entire assemblage, and schematically sketched in Fig. 15b (indicated with *pref. H_2O loss*, c.f. Fig. 10 in Doppler et al., 2013). The schematically illustrated horizontal arrows pointing to the left illustrate T_h modifications due to total volume loss, which is more efficient for smaller inclusions than for large inclusions. Small inclusions lose a larger fraction of their total volume than large inclusions, because the latter have a smaller surface to volume ratio, given identical shapes. Consequently, smaller inclusions may reveal a much larger variety of T_h values according to the two simultaneously operating processes, than large inclusions.

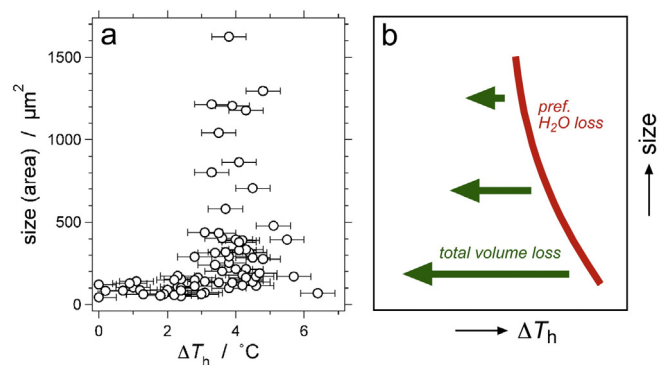


Fig. 15. (a) Diagram of T_h modification (ΔT_h) versus inclusion size, represented by its area in μm^2 in two dimensional projections from R-005a. (b) Diagram schematically illustrating the effects of the processes (1) preferential H_2O loss (red) and (2) total volume loss (green) according to theoretical considerations. The length of the green arrows illustrates that large inclusions are less affected by this process than small inclusions. (For interpretation of the references to color in this figure legend, the reader is referred to the web version of this article.)

4.6. Re-equilibration experiment R-011a and R-014a

The conditions of re-equilibration R-011a and R-014a are similar to the previously described experiments R-005a, b, and c. The original synthesis produced fluid inclusion assemblages with variable underpressures (c.f. Figs. 6b and 7b), and therefore, both H₂O fugacity gradients and pressure gradients are present at the start of re-equilibration. Re-equilibration experiments with 10 and 16.3 mass% NaCl aqueous fluid inclusions, R-011a and R-014a, respectively, result in increased salinities of individual fluid inclusions, but opposite adjustments of T_h 's. Similar to calculated modifications for R-005a, b, and c, these re-equilibration experiments also reveal a preferential loss of H₂O in addition to total volume loss (Fig. 13), despite the converse modifications of T_h 's. The re-equilibration experiments of 458 to 460 h correspond to similar percentages of preferential loss of the amount of H₂O and total volume loss (c.f. R-005a and R-011a), whereas approximately twice as much loss is observed for the experiments at 960 to 962 h (c.f. R-005b and R-014a).

All experiments with H₂O–NaCl fluid inclusions reveal similar modifications according to preferential H₂O loss and total volume loss, and the magnitude of modification is time-dependent. Diffusion of fluid species through quartz according to fugacity gradients is not the major process that may adjust fluid compositions and densities in fluid inclusions.

4.7. Natural fluid inclusions

Knowledge of the behavior of synthetic fluid inclusions in re-equilibration experiments is the major tool in understanding fluid modifications in natural fluid inclusions that have suffered abundant gradients in pressure and fugacity after entrapment during the long exhumation history of rock. The possibilities of modification of natural fluid inclusions are numerous, therefore, we may better identify geological conditions that do not modify inclusions. However, the analyzed fluid properties themselves are usually the main arguments for the preservation of deep fluids.

Post-entrapment modifications of natural fluid inclusions have so far mainly been derived from textural evidence, notably the shape of individual fluid inclusions (e.g. Ayllón et al., 2003). The effects of diffusion are difficult to recognize in rock because it may not leave observable traces in the sample. Diffusion can be interpreted from a fluid inclusion assemblage with variable fluid properties. Because diffusion does not affect all fluid inclusions in one assemblage with similar far-reaching modifications (e.g. Doppler et al., 2013), reconstruction calculation is possible by comparing the properties of the remaining fluid species in individual inclusions. For example, Table 6 illustrates a variety of possible T_h – T_m pairs in individual H₂O–NaCl-rich inclusions that resulted from specific amounts of preferential H₂O loss. These reconstruction calculations can also be performed for H₂O–gas-rich fluid inclusions. For example, an inclusion with originally 50 vol.% aqueous liquid phase, and CO₂ phases that homogenize at +25.0 °C in the liquid phase: after 10 amount% preferential H₂O loss by diffusion, the vol.% is modified to 45% whereas T_h (CO₂) is modified to +28.2 °C. A set of combined vol.% and T_h (CO₂) of individual inclusions allow reconstruction of an originally homogeneous fluid inclusion assemblage. Similar reconstruction calculations were performed for experimentally re-equilibrated natural H₂O–CO₂–NaCl-rich fluid inclusions by Baumgartner et al. (2014).

Preferential H₂O loss seems to be a general process in modifications of fluid inclusions in all experimental and natural settings, and was also evidenced in deformation experiments with natural fluid inclusions (Diamond et al., 2010). This process occurs in hydrostatic experiments as well as in experiments with differential stresses, and is the main factor to modify both inclusion composition and density.

Our study illustrates that inclusions with only minor gradients in fugacity and pressure are modified by preferential H₂O loss, similar to the considerations of Bakker and Jansen (1990, 1991, 1994), and that the

host crystal has the tendency to expel the enclosed fluid inclusions by internal accretion. These results suggest that high salinity natural fluid inclusions, which are formed at high temperature and pressure conditions (e.g. in an igneous environment) are most probably modified by preferential H₂O loss. The presence of abundant entrapped crystals in fluid inclusions that are not able to homogenize at high temperatures, may have resulted from preferential H₂O loss and total volume loss. The properties of an originally homogeneous natural fluid inclusion assemblage can always be reconstructed by thermodynamic modeling if only preferential H₂O loss and total volume loss are considered according to the abovementioned considerations.

Acknowledgments

We would like to thank the Austrian Science Fund (FWF) for the financial support (project no. P 22446-N21). Larry Diamond and Thomas Pettke are acknowledged for their critical and constructive reviews.

Appendix A. Supplementary data

Supplementary data to this article can be found online at <http://dx.doi.org/10.1016/j.chemgeo.2016.01.014>.

References

- Anderko, A., Pitzer, K.S., 1993. Phase equilibria and volumetric properties of the system KCl–H₂O and NaCl–KCl–H₂O above 573 K: equation of state representation. *Geochim. Cosmochim. Acta* 57, 4885–4897.
- Audétat, A., Günther, D., 1999. Mobility and H₂O loss from fluid inclusions in natural quartz crystals. *Contrib. Mineral. Petrol.* 137, 1–14.
- Ayllón, F., Bakker, R.J., Warr, L.N., 2003. Re-equilibration of fluid inclusions in diagenetic anchizonal rocks of the Cifera–Matallana coal basin (NW Spain). *Geofluids* 3, 49–68.
- Bakker, R.J., 2003. Package FLUIDS 1. Computer programs for analysis of fluid inclusion data and for modelling bulk fluid properties. *Chem. Geol.* 194, 3–23.
- Bakker, R.J., 2004. Raman spectra of fluid and crystal mixtures in the systems H₂O, H₂O–NaCl, and H₂O–MgCl₂ at low temperatures: applications to fluid inclusion research. *Can. Mineral.* 42, 1283–1314.
- Bakker, R.J., 2009. Re-equilibration of fluid inclusions: bulk diffusion. *Lithos* 112, 277–288.
- Bakker, R.J., 2011. The use of quantities, units and symbols in fluid inclusion research. *Berichte der Geologischen Bundesanstalt* 87, pp. 5–11.
- Bakker, R.J., 2012. Package FLUIDS. Part 4: thermodynamic modelling and purely empirical equation of state for H₂O–NaCl–KCl solutions. *Mineral. Petrol.* 105, 1–29.
- Bakker, R.J., Jansen, J.B.H., 1990. Preferential water leakage from fluid inclusions by means of mobile dislocations. *Nature* 345, 58–60.
- Bakker, R.J., Jansen, J.B.H., 1991. Experimental post-entrapment water loss from synthetic CO₂–H₂O inclusions in natural quartz. *Geochim. Cosmochim. Acta* 55, 2215–2230.
- Bakker, R.J., Jansen, J.B.H., 1994. A mechanism for preferential H₂O leakage from fluid inclusions in quartz, based on TEM observations. *Contrib. Mineral. Petrol.* 116, 7–20.
- Bakker, R.J., Diamond, L.W., 2006. Estimation of volume fractions of liquid and vapor phases in fluid inclusions, and definition of inclusion shapes. *Am. Mineral.* 91, 635–657.
- Bakker, R.J., Elburg, M.A., 2006. A magmatic-hydrothermal transition in Arkaroola (northern Flinders Ranges, South Australia): from diopside–titanite pegmatites to hematite–quartz growth. *Contrib. Mineral. Petrol.* 152, 541–569.
- Barker, A.J., 1995. Post-entrapment modification of fluid inclusions due to overpressure: evidence from natural samples. *J. Metamorphic Geol.* 13, 737–750.
- Baumgartner, M., Bakker, R.J., Doppler, G., 2014. Re-equilibration of natural H₂O–CO₂–salt-rich fluid inclusions in quartz – part 1: experiments in pure water at constant pressures and differential pressures at 600 °C. *Contrib. Mineral. Petrol.* 168, 1017.
- Bodnar, R.J., Sterner, S.M., 1987. Synthetic fluid inclusions. In: Barnes, H.L., Ulmer, G.C. (Eds.), *Hydrothermal Experimental Techniques*. Wiley, New York, pp. 423–457.
- Cherniak, D.J., 2003. Silicon self-diffusion in single-crystal natural quartz and feldspar. *Earth Planet. Sci. Lett.* 214, 655–668.
- Diamond, L.W., Tarantola, A., Stünitz, H., 2010. Modification of fluid inclusions in quartz by deviatoric stress. II: experimentally induced changes in inclusion volume and composition. *Contrib. Mineral. Petrol.* 160, 845–864.
- Doppler, G., 2014. Experimental Study of Fluid Inclusion Re-equilibration in Quartz (Dissertation) Montanuniversität Leoben, Austria, p. 137.
- Doppler, G., Bakker, R.J., 2014. The influence of the α – β phase transition of quartz on fluid inclusions during re-equilibration experiments. *Lithos* 198–199, 14–23.
- Doppler, G., Bakker, R.J., Baumgartner, M., 2013. Fluid inclusion modification by H₂O and D₂O diffusion: the influence of inclusion depth, size, and shape in re-equilibration experiments. *Contrib. Mineral. Petrol.* 165, 1259–1274.
- Driesner, T., 2007. The system H₂O–NaCl. Part II. Correlation for molar volume, enthalpy, and isobaric heat capacity from 0 to 1000 °C, 1 to 5000 bar, and 0 to 1 xNaCl. *Geochim. Cosmochim. Acta* 71, 4902–4919.

- Driesner, T., Heinrich, C.A., 2007. The system H_2O – NaCl . Part I. Correlation formulae for phase relations in the temperature–pressure–composition space from 0 to 1000 °C, 0 to 5000 bar, and 0 to 1 xNaCl. *Geochim. Cosmochim. Acta* 71, 4880–4901.
- Haar, L., Gallagher, J.S., Kell, G.S., 1984. NBS/NRC Steam Tables. Hemisphere Publishing Corporation, Washington.
- Hosieni, K.R., Howald, R.A., Scanlon, M.W., 1985. Thermodynamics of the lambda transition and the equation of state of quartz. *Am. Mineral.* 70, 782–793.
- Johnson, E.A., 2006. Water in nominally anhydrous crustal minerals: speciation, concentration, and geologic significance. In: Keppler, H., Smyth, R. (Eds.), *Water in Nominally Anhydrous Minerals*. Reviews in Mineralogy vol. 62, pp. 117–154.
- Kerrick, D.M., 1987. Cold-seal systems. In: Ulmer, G.C., Barnes, H.L. (Eds.), *Hydrothermal Experimental Techniques*. Wiley, New York, pp. 293–323.
- Küster, M., Stöckert, B., 1997. Density changes of fluid inclusions in high-pressure low-temperature metamorphic rocks from Crete: a thermobarometric approach based on creep strength of the host minerals. *Lithos* 41, 151–167.
- Pettke, T., Oberli, F., Audetat, A., Guillong, M., Simon, A.C., Hanley, J.J., Klemm, L.M., 2012. Recent developments in element concentration and isotope ratio analyses of individual fluid inclusions by laser ablation single and multiple collector ICP-MS. *Ore Geol. Rev.* 44, 10–38.
- Roedder, E., 1984. Fluid inclusions. *Mineral. Soc. Am. Rev. Mineral.* 12, 644.
- Samson, I., Anderson, A., Marshall, D., 2003. Fluid inclusions: analysis and interpretation. *Mineral. Assoc. Can. Short Course* 32, 370.
- Sterner, S.M., Bodnar, R.J., 1989. Synthetic fluid inclusions – VII. Re-equilibration of fluid inclusions in quartz during laboratory-simulated metamorphic burial and uplift. *J. Metamorph. Geol.* 7, 243–260.
- Sterner, S.M., Hall, D.L., Keppler, H., 1995. Compositional re-equilibration of fluid inclusions in quartz. *Contrib. Mineral. Petrol.* 119, 1–15.
- Vityk, M.O., Bodnar, R.J., 1995. Textural evolution of synthetic fluid inclusions in quartz during reequilibration, with applications to tectonic reconstruction. *Contrib. Mineral. Petrol.* 121, 309–323.
- Vityk, M.O., Bodnar, R.J., 1998. Statistical microthermometry of synthetic fluid inclusions in quartz during decompression reequilibration. *Contrib. Mineral. Petrol.* 132, 149–162.
- Zhang, Y.G., Frantz, J.D., 1987. Determination of the homogenization temperatures and densities of supercritical fluids in the system NaCl – KCl – CaCl_2 – H_2O using synthetic fluid inclusions. *Chem. Geol.* 64, 335–350.

Appendix A

GMR-004d

Inclusion	Depth / μm		Area (pixel)*	Perimeter (pixel)*	Best-fit Ellips		$T_m / ^\circ\text{C}$ SV \rightarrow LV	$T_h / ^\circ\text{C}$ LV \rightarrow L
	from Bottom	from Top			Major axis	Minor axis		
F11	12	29	17140	823	379	58	0,0	292,7
F12	9	43	10480	382	137	98	0,0	292,8
F13	8	151	8240	356	105	100	-	292,8
F14	74	36	10877	377	128	108	-	292,4
F15	74	50	9744	359	121	103	-	291,8
F16	59	104	25978	732	333	99	-	292,7
F17	66	104	9668	371	145	85	-	292,7
F18	62	155	18472	565	240	98	-	292,9
F19	66	140	6408	329	137	60	-	293,1
F110	29	198	25440	590	210	155	-	293,8
F111	22	277	22882	907	362	80	-	292,4
F112	5	482	11503	397	149	98	-	293,0
F113	15	490	22055	532	170	165	-	293,0
F114	15	486	15284	465	178	110	-	293,0
F115	96	389	17955	754	264	87	-	294,3
F116	103	389	10482	615	225	59	-	292,4
F117	97	324	20162	766	330	78	-	293,3
F118	22	288	31839	1038	399	102	-	295,6
F119	17	194	33854	723	290	149	-	293,5
F120	82	76	31126	897	305	130	-	292,5
F121	29	79	25107	617	238	134	-	292,3
F122	22	83	11137	396	133	106	-	293,0
F123	34	43	18618	520	197	120	-	292,7
F124	22	490	74025	1276	537	175	-	292,7
F125	120	868	67041	1501	398	215	-	292,9
F126	165	994	15009	628	241	79	-	293,6
F127	35	936	14704	448	162	115	-	292,6
F128	23	900	43288	1339	569	97	-	293,4
F129	12	803	30832	701	273	144	-	292,7
F130	26	738	101494	2692	1230	105	-	-
F131	154	648	18381	574	250	94	-	292,7
F132	161	752	14047	773	364	49	-	292,5
F133	137	407	11190	410	158	90	-	292,4
F134	147	360	14924	568	259	73	-	292,7
F135	198	529	17303	553	231	96	-	291,2
F136	198	544	41504	1146	561	94	-	290,6
F137	251	418	31219	716	267	149	-	291,6
F138	239	367	34087	777	324	134	-	291,0
F139	177	310	58163	1418	715	104	-	291,2
F140	172	263	8711	437	204	54	-	292,7
F141	248	259	18032	530	205	112	-	292,7
F142	216	295	13002	429	148	112	-	292,7
F143	194	187	25280	1090	505	64	-	292,9
F144	224	101	13015	465	194	85	-	292,3
F145	184	72	19397	566	213	116	-	293,3
F146	151	112	18984	556	227	107	-	293,1
F147	116	198	23073	777	288	102	-	292,5
F148	5	144	14964	575	272	70	-	292,5
F149	29	68	12903	534	247	66	-	294,1
F150	93	58	16701	488	182	117	-	292,7
F151	160	162	31437	1000	310	129	-	292,7
F152	141	18	11729	404	140	107	-	292,1
F153	141	14	8765	344	125	89	-	291,6
F154	141	43	11672	391	140	106	-	291,6
F155	151	29	23812	722	288	105	-	292,1
F156	151	58	12819	419	151	108	-	292,3
F157	109	202	25819	591	196	168	-	292,5
F158	166	61	21138	525	181	149	-	293,0
F159	107	140	6818	330	136	64	-	292,1
F160	97	140	9050	352	122	94	-	293,1
F161	32	155	13913	457	185	96	-	293,6
F162	222	86	37216	983	406	117	-	292,8
F163	269	194	15866	739	284	71	-	292,6
F164	199	349	48815	983	429	145	-	292,8
F165	166	702	68951	1028	349	252	-	293,0
F166	273	749	22648	546	186	155	-	292,9
F167	154	529	85205	1181	481	226	-	293,0
F168	189	428	37423	1208	601	79	-	292,1
F169	188	360	25239	636	243	132	-	292,6
F170	161	148	22472	555	204	140	-	292,1
F171	108	698	26419	626	249	135	-	290,7
F172	176	803	10795	463	192	72	-	291,5
F173	176	731	7146	342	135	67	-	292,3
F174	221	796	10643	515	235	58	-	292,6
F175	156	396	94356	2124	571	210	-	292,4
F176	207	436	22042	586	242	116	-	292,4
F177	248	338	47853	1098	437	140	-	292,3
F178	257	328	12020	399	138	111	-	-
F179	253	310	16174	497	196	105	-	292,2
F180	240	295	15523	458	167	118	-	292,3
F181	270	25	39021	869	360	138	-	292,3
F182	270	29	14028	492	183	97	-	292,7
F183	224	108	29608	639	240	157	-	290,3
F184	224	122	17050	564	250	87	-	290,8
F185	167	234	68470	1341	642	136	-	292,7
F186	105	266	23912	1153	422	72	-	291,1
F187	111	292	10289	400	163	81	-	291,9
F188	269	133	36614	991	270	173	-	292,4
F189	264	86	33686	1576	528	81	-	292,2
F190	184	76	45482	1579	354	164	-	-
F191	176	176	88988	2229	1003	113	-	293,2
F192	221	158	54814	1023	426	164	-	292,5
F193	259	101	14091	439	151	119	-	292,9
F194	269	43	12961	447	164	101	-	291,8
F195	259	40	16265	482	189	109	-	290,9
F196	57	97	49326	1039	446	141	-	292,1
F197	99	22	28795	1090	364	101	-	291,8
F198	91	65	17574	994	222	101	-	289,5
F199	105	180	24590	730	334	94	-	292,7
F1100	99	151	15061	451	163	117	-	292,6

(pixel)* 1 μm = 15.83 pixel

excluded data, lost fluid inclusions after re-equilibration

R-004d

Inclusion	Area (pixel)*	Perimeter (pixel)*	Best-fit Ellips		$T_m / ^\circ\text{C}$ SV \rightarrow LV	$T_h / ^\circ\text{C}$ LV \rightarrow L
			Major axis	Minor axis		
F11	-	-	-	-	-	-
F12	-	-	-	-	-	-
F13	-	-	-	-	-	-
F14	10607	370	124	109	0,0	294,4
F15	9814	360	121	104	0,0	293,8
F16	24319	653	287	108	0,0	294,8
F17	10195	380	148	88	0,0	294,8
F18	17142	515	212	103	0,0	295,1
F19	5597	286	113	63	0,0	296,3
F110	-	-	-	-	-	-
F111	-	-	-	-	-	-
F112	-	-	-	-	-	-
F113	-	-	-	-	-	-
F114	-	-	-	-	-	-
F115	-	-	-	-	-	-
F116	-	-	-	-	-	-
F117	-	-	-	-	-	-
F118	-	-	-	-	-	-
F119	-	-	-	-	-	-
F120	24420	585	197	158	0,1	294,5
F121	-	-	-	-	-	-
F122	-	-	-	-	-	-
F123	-	-	-	-	-	-
F124	-	-	-	-	-	-
F125	-	-	-	-	-	-
F126	-	-	-	-	-	-
F127	-	-	-	-	-	-
F128	-	-	-	-	-	-
F129	-	-	-	-	-	-
F130	-	-	-	-	-	-
F131	-	-	-	-	-	-
F132	-	-	-	-	-	-
F133	11789	409	158	95	0,0	294,3
F134	14345	509	222	82	0,0	294,6
F135	16737	526	220	97	0,0	293,5
F136	42837	1044	500	109	0,0	292,6
F137	32617	690	257	161	0,0	293,6
F138	33496	736	302	141	0,1	293,1
F139	53631	1348	678	101	0,1	293,2
F140	7767	404	184	54	0,0	295,2
F141	17286	509	199	110	0,0	294,5
F142	12791	412	144	113	0,0	294,5
F143	24724	743	344	92	0,0	294,8
F144	13127	433	158	105	0,1	294,6
F145	17067	494	174	125	0,0	295,3
F146	18954	533	214	113	0,1	295,0
F147	20543	558	228	115	0,0	294,4
F148	-	-	-	-	-	-
F149	-	-	-	-	-	-
F150	15491	458	171	116	0,0	294,6
F151	18117	517	170	135	0,1	294,8
F152	11158	388	134	106	0,1	294,3
F153	8793	343	125	89	0,1	293,7
F154	11246	387	142	101	0,1	293,7
F155	19397	555	223	111	0,0	293,9
F156	10220	363	121	108	0,0	294,3
F157	23810	559	192	158	0,1	294,3
F158	19231	497	163	150	0,0	294,8
F159	7283	328	132	70	0,0	294,5
F160	8150	333	117	89	0,0	295,5
F161	-	-	-	-	-	-
F162	35756	806	358	127	0,1	294,6
F163	82715	1342	553	191	0,0	294,8
F164	49334	936	409	153	0,1	294,8
F165	62810	963	361	222	0,0	294,9
F166	22526	543	187	154	0,0	294,7
F167	85085	1157	464	234	0,0	294,8
F168	32972	1093	534	79	0,0	294,7
F169	26777	636	243	140	0,1	294,5
F170	23609	569	212	142	0,1	293,9
F171	25724	604	235	139	0,0	292,7
F172	11282	412	168	85	0,0	293,9
F173	6764	316	122	71	0,1	294,2
F174	9738	438	200	62	0,1	294,6
F175	70420	993	363	247	0,0	294,3
F176	48683	881	356	174	0,1	294,2
F177	47481	850	334	181	0,0	294,2
F178	11828	393	136	111	-	-
F179	15541	473	183	108	0,0	294,4
F180	15283	450	162	120	0,0	294,4
F181	31062	670	264	150	0,1	294,3
F182	12244	404	144	108	0,1	294,9
F183	27614	609	217	162	0,0	292,4
F184	17583	540	223	100	0,0	293,0
F185	51780	982	429	154	-	295,5
F186	15474	466	175	113	-	-
F187	9639	368	140	88	-	294,0
F188	28248	633	232	155	-	294,2
F189	21229	992	338	80	-	294,8
F190	35146	897	244	184	-	-
F191	52224	1025	470	141	-	297,6
F192	44285	810	324	174	-	294,5
F193	12708	407	136	119	-	294,9
F194	12230	411	148	105	-	294,0
F195	16073	460	163	126	-	292,9
F196	27316	698	292	119	-	294,2
F197	-	-	-	-	-	-
F198	11539	402	150	98	-	292,3
F199	21966	624	274	102	-	295,1
F1100	14066	429	149	120	-	294,7

Appendix A

GMR-004g								R-004g							
Inclusion	Depth / μm		Area (pixel)*	Perimeter (pixel)*	Best-Fit Ellips		$T_m / ^\circ\text{C}$ SV \rightarrow LV	$T_b / ^\circ\text{C}$ LV \rightarrow L	Inclusion	Area (pixel)	Perimeter (pixel)	Best-Fit Ellips		$T_m / ^\circ\text{C}$ SV \rightarrow LV	$T_b / ^\circ\text{C}$ LV \rightarrow L
	from Top	from Side			Major axis	Minor axis						Major axis	Minor axis		
F11	6	13	36209	1169	359	126	-	293.7	F11	144439	2017	632	291	-	292.6
F12	15	29	2754	194	68	52	-	293.0	F12	12188	405	131	118	-	291.4
F13	23	11	8023	640	235	43	-	292.8	F13	28693	857	326	112	-	292.8
F14	25	11	3590	313	135	34	-	292.7	F14	14923	516	215	88	-	291.1
F15	25	35	3308	213	72	58	-	292.3	F15	14042	437	147	122	-	291.4
F16	3	33	2089	171	62	43	-	290.3	F16	10007	383	143	89	-	289.6
F17	5	33	2389	183	65	47	-	292.4	F17	10195	376	123	106	-	291.1
F18	5	55	4235	263	98	55	-	286.5	F18	15248	457	164	118	-	286.2
F19	11	77	2028	189	78	33	-	291.9	F19					-	291.3
F110	11	88	7115	312	107	84	-	292.9	F110	30466	656	236	164	-	292.2
F111	5	99	8495	344	122	89	-	293.2	F111	39788	736	250	202	-	292.6
F112	5	79	4863	373	176	35	-	292.6	F112	24712	776	355	89	-	292.4
F113	15	110	17633	579	257	87	-	292.2	F113	84082	1221	529	202	-	291.8
F114	32	132	24536	1320	462	68	-	293.2	F114	115791	2743	1017	145	-	292.8
F115	43	132	6367	529	273	30	-	292.6	F115	29929	1072	537	71	-	292.0
F116	54	106	6612	336	141	60	-	292.5	F116	27632	686	291	121	-	292.2
F117	73	51	14904	465	144	132	-	294.3	F117	65426	966	307	271	-	293.7
F118	43	154	20760	646	287	92	-	293.2	F118	97519	1376	605	205	-	292.5
F119	23	112	26493	780	287	118	-	292.8	F119	110199	1606	576	243	-	292.1
F120	34	35	9851	392	153	82	-	293.3	F120	46852	810	290	206	-	292.7
F121	3	242	101931	3308	1281	101	-	294.1	F121	405366	6535	2361	219	-	294.0
F122	12	312	21570	537	190	145	-	292.7	F122	96909	1134	400	308	-	292.4
F123	12	359	72606	2893	1261	73	-	293.0	F123	395684	6174	2614	193	-	292.4
F124	15	374	46235	1737	705	84	-	295.2	F124	197858	3553	1536	164	-	295.3
F125	15	288	68392	1219	549	159	0.0	294.3	F125	306005	2524	1149	339	0.0	294.6
F126	19	233	13581	466	190	91	-	292.9	F126	65392	992	394	211	-	292.1
F127	20	128	33771	704	247	174	-	294.2	F127	157097	1492	533	375	-	293.6
F128	14	106	34644	702	265	166	-	293.0	F128	162745	1507	563	368	-	292.5
F129	20	75	9584	377	151	81	-	293.1	F129	45673	840	337	173	-	292.5
F130	19	51	13295	420	144	117	-	292.7	F130	62386	910	306	259	-	292.0
F131	15	165	13341	439	161	105	-	292.4	F131	60781	933	329	235	-	291.4
F132	34	95	10086	528	245	52	-	292.6	F132	46245	1070	501	118	-	291.4
F133	31	55	26880	1338	622	55	-	293.1	F133	113218	2707	1276	113	-	292.0
F134	5	44	6613	311	103	81	-	292.8	F134	35063	782	267	167	-	292.3
F135	5	44	7613	365	134	72	-	292.3	F135	29146	668	227	163	-	291.6

(pixel)* 1 μm = 15.83 pixel
after re-equilibration experiment R-004g pixels are measured with different software

excluded data, or lost fluid inclusions after re-equilibration

Appendix A

GMR-005a

Inclusion	Depth / μm		Area μm^2	Perimeter μm	Best-Fit Ellips		Area vapour μm^2	$T_e / ^\circ\text{C}$		$T_m / ^\circ\text{C}$	$T_b / ^\circ\text{C}$
	from Bottom/Top	from Side			major (μm)	minor (μm)		SSV \rightarrow SLV	SLV \rightarrow LV		LV \rightarrow L
FI 1	125	81	394,3	76,3	30,2	16,6	94,9	-	-16,5	-	330,0
FI 2	97	101	88,1	35,8	12,1	9,3	21,1	-21,5 #	-16,6	-	330,3
FI 3	108	107	151,9	51,0	21,8	8,9	37,4	-21,5 #	-16,6	-	330,3
FI 4	45	174	120,2	39,9	13,8	11,1	31,2	-	-	-	330,1
FI 5	100	226	478,0	86,4	34,4	17,7	114,2	-21,5 #	-16,4	-	330,0
FI 6	133	269	863,7	113,9	41,8	26,3	190,5	-21,5 #	-16,4	-	329,7
FI 7	119	284	214,6	52,9	17,8	15,3	74,1	-21,5 #	-16,4	-	329,7
FI 8	111	284	216,5	58,5	23,5	11,7	51,2	-	-	-	329,9
FI 9	159	223	74,7	32,2	12,4	7,7	24,5	-	-1,2	-	287,8
FI 10	181	203	217,9	57,1	21,0	13,2	59,0	-	-1,3	-	276,8
FI 11	117	197	67,7	30,7	11,8	7,3	18,7	-	-	-	325,1
FI 12	179	177	161,7	51,2	21,7	9,5	41,2	-	-	-	330,5
FI 13	144	23	-	-	-	-	-	-	-	-	331,1
FI 14	103	20	-	-	-	-	-	-	-	-	331,4
FI 15	90	87	316,1	91,3	35,5	11,3	58,5	-	-	-	330,6
FI 16	86	69	99,2	36,4	12,7	9,9	25,2	-	-	-	331,9
FI 17	116	136	113,5	39,7	15,2	9,5	28,6	-	-	-	330,8
FI 18	139	255	1.205,8	142,5	45,1	34,0	205,6	-	-	-	324,8
FI 19	153	237	-	-	-	-	-	-	-	-	330,9
FI 20	139	396	-	-	-	-	-	-	-1,4	-	272,0
FI 21	137	197	402,8	92,1	35,4	14,5	92,2	-21,5 #	-16,5	-	332,8
FI 22	213	191	-	-	-	-	-	-	-	-	328,7
FI 23	145	148	132,6	42,9	16,4	10,3	29,9	-	-	-	331,9
FI 24	108	69	102,7	48,5	22,6	5,8	22,9	-	-	-	330,2
FI 25	150	278	387,9	107,2	49,3	10,0	68,3	-	-	-	330,7
FI 26	184	217	221,1	55,0	20,7	13,6	65,4	-	-	-	331,0
FI 27	182	379	579,6	88,9	31,9	23,2	146,3	-	-	-	330,9
FI 28	190	394	1.040,9	134,9	45,7	29,0	193,2	-21,5 #	-16,3	-	331,1
FI 29	171	556	437,4	75,4	26,0	21,4	124,3	-	-	-	330,0
FI 30	215	573	106,5	37,3	13,2	10,3	28,3	-	-	-	328,3
FI 31	157	98	140,5	57,8	24,0	7,5	26,2	-	-	-	332,6
FI 32	199	93	83,4	37,1	15,8	6,7	17,6	-21,5 #	-16,5	-	331,3
FI 33	184	75	43,5	24,1	8,5	6,5	10,3	-21,5 #	-16,5	-	331,8
FI 34	218	107	82,8	36,4	14,8	7,1	19,8	-	-	-	330,5
FI 35	192	78	86,0	33,6	11,5	9,5	18,4	-	-	-	331,2
FI 36	178	162	285,5	82,3	39,1	9,3	55,3	-	-	-	329,6
FI 37	103	281	141,6	44,2	15,9	11,3	29,8	-	-	-	330,9
FI 38	69	437	147,6	51,2	22,5	8,4	28,5	-	-	-	331,2
FI 39	163	695	241,6	57,4	19,2	16,1	45,8	-	-	-	330,7
FI 40	140	825	254,7	85,0	34,0	9,5	40,0	-	-	-	329,1
FI 41	66	585	343,2	67,2	21,7	20,1	93,9	-	-1,4	-	290,4
FI 42	159	619	-	-	-	-	-	-	-1,4	-	292,1
FI 43	159	582	71,5	30,9	11,2	8,1	16,0	-	-	-	329,1
FI 44	191	541	1.214,9	127,4	44,7	34,6	308,2	-	-	-	330,7
FI 45	190	535	152,8	62,1	26,0	7,5	34,2	-	-	-	329,1
FI 46	202	718	142,6	54,1	24,3	7,5	36,2	-	-2,3	-	291,3
FI 47	218	880	215,2	56,7	22,8	12,0	48,6	-	-	-	329,2
FI 48	173	929	292,7	62,2	21,2	17,6	92,1	-	-	-	330,7
FI 49	222	813	394,5	86,4	36,8	13,7	90,2	-	-	-	328,9
FI 50	187	1007	1.296,8	141,9	56,6	29,2	318,0	-	-	-	327,4
FI 51	182	1071	1.177,4	134,1	52,6	28,5	232,5	-	-	-	328,0
FI 52	161	706	335,0	67,4	24,5	17,4	97,5	-	-	-	326,2
FI 53	201	1007	319,0	93,2	33,1	12,3	63,6	-	-	-	324,4
FI 54	211	1227	330,4	69,0	26,8	15,7	90,0	-	-	-	330,5
FI 55	222	1317	390,5	104,8	49,2	10,1	75,0	-	-	-	331,4
FI 56	201	1108	313,8	76,9	33,6	11,9	68,6	-	-	-	328,7
FI 57	109	1013	802,1	105,6	39,6	25,8	187,7	-	-	-	330,9
FI 58	181	1100	80,8	32,4	10,7	9,6	22,4	-21,5 #	-16,6	-	332,3
FI 59	181	1042	99,7	38,3	14,0	9,1	27,9	-21,5 #	-16,6	-	332,1
FI 60	132	955	110,1	52,9	25,5	5,5	23,7	-	-	-	330,9
FI 61	202	382	290,5	65,4	21,9	16,9	60,9	-	-	-	331,1
FI 62	161	382	50,3	26,1	9,6	6,7	11,7	-	-	-	330,8
FI 63	161	420	56,5	28,1	10,7	6,7	13,0	-	-	-	330,2
FI 64	47	252	-	-	-	-	-	-	-	-	329,9
FI 65	143	457	139,0	55,8	25,7	6,9	29,5	-	-	-	329,0
FI 66	40	38	-	-	-	-	-	-	-	-	328,5
FI 67	77	214	-	-	-	-	-	-	-	-	328,7
FI 68	11	339	-	-	-	-	-	-	-	-	328,8
FI 69	22	454	-	-	-	-	-	-	-	-	330,0
FI 70	42	20	-	-	-	-	-	-	-	-	328,2
FI 71	56	14	-	-	-	-	-	-	-	-	328,7
FI 72	57	29	-	-	-	-	-	-	-	-	328,5
FI 73	155	130	-	-	-	-	-	-	-	-	329,7
FI 74	196	324	-	-	-	-	-	-	-	-	328,9
FI 75	215	127	-	-	-	-	-	-	-	-	328,5
FI 76	11	156	276,7	73,3	31,5	11,2	54,4	-21,5 #	-16,4	-	329,6
FI 77	11	153	131,7	49,9	21,3	7,9	27,0	-21,5 #	-16,4	-	329,5
FI 78	39	240	202,0	52,5	19,5	13,2	48,5	-	-	-	329,5
FI 79	105	443	168,7	48,4	18,1	11,9	37,9	-	-	-	328,6
FI 80	125	402	127,6	58,6	28,5	5,7	25,7	-	-	-	329,1
FI 81	127	313	379,3	116,3	48,4	10,0	67,0	-	-	-	329,5
FI 82	136	249	178,4	60,0	21,0	10,8	35,7	-	-	-	329,5
FI 83	117	93	172,9	50,2	17,2	12,8	37,5	-	-	-	329,1
FI 84	26	162	-	-	-	-	-	-	-	-	329,1
FI 85	106	107	147,9	59,3	27,3	6,9	31,4	-	-	-	331,0
FI 86	31	162	61,8	29,0	10,7	7,4	16,6	-	-	-	328,7
FI 87	46	130	83,2	32,8	11,0	9,6	21,8	-21,5 #	-16,5	-	327,9
FI 88	52	159	84,8	35,1	13,9	7,8	20,0	-21,5 #	-16,5	-	327,9
FI 89	66	214	63,3	29,0	10,0	8,0	16,2	-	-	-	329,5
FI 90	51	281	135,6	43,8	16,7	10,3	36,2	-	-	-	328,7
FI 91	34	344	161,3	47,4	18,2	11,3	44,3	-21,5 #	-16,5	-	328,6
FI 92	31	362	115,0	39,5	14,7	10,0	32,0	-21,5 #	-16,6	-	328,6
FI 93	26	391	168,9	47,6	17,0	12,6	43,3	-21,5 #	-16,6	-	328,6
FI 94	34	341	53,5	26,2	8,6	7,9	14,5	-	-	-	329,5
FI 95	17	344	63,2	30,5	12,3	6,5	16,7	-	-	-	327,7
FI 96	13	451	3.844,5	263,7	100,4	48,8	753,1	-	-	-	330,2
FI 97	13	370	1.623,7	176,0	70,2	29,4	364,6	-	-	-	330,2
FI 98	19	449	191,0	52,0	19,5	12,5	36,9	-	-	-	330,5
FI 99	10	394	433,5	83,8	34,1	16,2	91,0	-	-	-	330,5
FI 100	43	275	704,7	137,1	53,9	16,6	147,5	-21,5 #	-16,5	-	330,7

primary fluid inclusions

uncertain data

Eutectic temperature is varying between -21.5 and -21.1 $^\circ\text{C}$, and may not correspond to the final dissolution temperature of hydrohalite at -21.1 $^\circ\text{C}$
First recrystallisation during heating occurs at about - 21.5 $^\circ\text{C}$, and can be mistaken for the eutectic temperature.

Appendix A

R-005a

Inclusion	Area µm²	Perimeter µm	Best-Fit Ellips		Area vapour µm²	T _n / °C	T _{rest} / °C	T _m / °C hydrohalite	T _m / °C SLV → LV	second T _m / °C SLV → LV	T _b / °C LV → L	second T _b / °C LV → L
			major (µm)	minor (µm)								
FI 1	373,4	72,5	28,3	16,8	93,0	-	-	-	-19,7		335,5	
FI 2	84,0	33,3	11,4	9,3	21,9	-	-	-	-18,9		332,3	
FI 3	140,1	48,4	20,5	8,7	35,5	-	-	-	-19,5		334,6	
FI 4	109,0	37,7	12,9	10,8	34,1	-	-	-	-18,0		330,1	
FI 5	451,0	83,1	33,1	17,3	-	-	-	-	-19,3		335,1	
FI 6	832,2	108,9	40,2	26,4	-	-	-	-	-18,7		333,8	
FI 7	208,5	52,3	17,8	14,9	68,1	-64	-26,6	-24,4	-19,1	-19,0	334,0	
FI 8	203,4	55,7	22,0	11,8	47,4	-65	-27,6	-25,5	-19,0	-19,1	334,2	
FI 9	72,1	31,9	12,5	7,4	21,4	-	-	-	-		-	
FI 10	210,9	56,2	20,8	12,9	58,1	-	-	-	-		-	
FI 11	68,8	30,9	11,9	7,4	19,7	-64	-28,0	-26,0	-17,7	-17,7	331,5	
FI 12	155,8	49,9	20,9	9,5	38,8	-	nd	nn	-19,1	-19,2	333,4	
FI 13	-	-	-	-	-	-	nd	nn	-18,5		332,7	
FI 14	-	-	-	-	-	-	nd	nn	-19,6		335,7	
FI 15	291,9	80,6	34,4	10,8	62,4	-65	nd	nn	-19,5		335,0	
FI 16	92,4	35,1	12,2	9,6	-	-	nd	nn	-19,5		335,7	
FI 17	106,4	38,7	15,0	9,0	-	-	nd	nn	-19,6		335,4	
FI 18	1.139,7	131,7	45,1	32,2	223,1	-64	-28,7	-24,3	-18,5	-18,2	328,7	
FI 19	-	-	-	-	-	-	nd	nn	-18,7		335,0	
FI 20	-	-	-	-	-	-	-	-	-		-	
FI 21	406,4	88,9	37,0	14,0	91,6	-65	nd	nn	-18,8	-18,9	336,4	
FI 22	-	-	-	-	-	-	-27,5	-23,9	-18,8	-18,9	332,9	
FI 23	120,7	40,7	15,4	10,0	30,3	-	nd	nn	-19,3		335,4	
FI 24	94,1	46,2	21,9	5,5	21,1	-	nd	nn	-18,7		331,2	
FI 25	371,9	101,3	46,7	10,1	66,5	-	nd	nn	-19,3		334,8	
FI 26	212,9	54,1	20,5	13,2	64,7	-	nd	nn	-19,1		334,8	
FI 27	560,5	87,4	31,4	22,7	143,7	-	-26,2	-23,6	-18,5	-18,6	334,6	
FI 28	973,6	125,8	44,0	28,2	190,8	-65,5	-26,3	-24,0	-18,7	-18,7	334,6	
FI 29	431,9	74,8	25,7	21,4	124,3	-65	-27,2	-23,7	-18,5	-18,5	333,1	
FI 30	102,9	36,9	13,3	9,9	30,6	-	-	-	-18,3		330,6	
FI 31	128,6	50,0	20,2	8,1	25,7	-64	nd	nn	-18,5		333,7	
FI 32	79,5	36,3	15,5	6,5	17,4	-	nd	nn	-18,8		332,0	
FI 33	43,0	23,9	8,5	6,5	10,1	-	nd	nn	-18,6		331,8	
FI 34	78,0	33,9	13,5	7,3	18,8	-	nd	nn	-18,6		330,7	
FI 35	82,2	32,8	11,4	9,2	18,6	-	nd	nn	-18,9		332,4	
FI 36	278,3	80,1	37,8	9,4	57,2	-	nd	nn	-19,5		334,1	
FI 37	137,1	43,3	15,6	11,2	30,3	-	nd	nn	-19,7		335,2	
FI 38	142,5	50,3	22,1	8,2	29,2	-	nd	nn	-19,2		334,0	
FI 39	238,9	56,9	18,8	16,2	51,1	-	nd	nn	-19,2		334,1	
FI 40	239,5	76,8	30,5	10,0	44,8	-	nd	nn	-19,2		332,9	
FI 41	330,7	65,8	21,5	19,6	93,7	-	-	-	-		-	
FI 42	-	-	-	-	-	-	-	-	-		-	
FI 43	67,7	30,1	10,9	7,9	17,2	-	nd	nn	-19,0		332,2	
FI 44	1.201,9	126,6	44,5	34,4	317,3	-64,8	-25,6	-23,5	-18,1	-18,4	334,0	
FI 45	144,8	59,6	25,0	7,4	32,4	-	nd	nn	-18,8		331,5	
FI 46	136,1	52,7	23,8	7,3	37,0	-	-	-	-		-	
FI 47	211,8	54,9	21,5	12,5	46,3	-	nd	nn	-19,5		333,2	
FI 48	282,8	61,2	21,2	17,0	77,7	-	-26,7	-24,8	-19,0	-19,0	334,5	
FI 49	386,2	83,7	35,5	13,9	85,1	-65	nd	nn	-18,9		332,9	
FI 50	1.312,9	146,1	58,7	28,5	308,3	-	-24,3	-22,8	-17,2	-17,4	332,2	
FI 51	1.201,9	136,3	54,4	28,1	253,8	-	-27,4	-24,9	-18,7	-18,9	332,3	
FI 52	315,7	65,7	24,1	16,7	87,0	-63,5	-28,4	-25,9	-18,1	-18,1	330,5	
FI 53	283,0	71,2	30,2	11,9	60,3	-64	-30,5	-26,3	-19,1	-19,1	328,1	
FI 54	325,9	68,5	26,3	15,7	84,4	-65	-27,0	-24,4	-19,3	-19,1	334,6	
FI 55	355,6	94,0	44,9	10,1	72,5	-	-27,5	-24,8	-19,2	-19,2	335,6	
FI 56	305,7	73,9	31,9	12,2	60,0	-64,5	-36,0	-25,6	-19,4	-19,1	332,1	
FI 57	798,2	105,2	39,2	25,9	212,8	-64	-25,5	-23,6	-18,5	-18,3	334,2	
FI 58	80,1	32,3	10,6	9,6	21,0	-	nd	nn	-18,7		334,7	
FI 59	103,0	39,1	14,0	9,4	28,2	-	nd	nn	-18,7		334,5	
FI 60	102,6	52,2	25,2	5,2	23,5	-	-27,0	-23,8	-18,7	-18,6	333,7	
FI 61	289,1	64,5	21,5	17,1	63,2	-64	nd	nn	-18,4		333,9	
FI 62	42,8	25,4	10,2	5,3	9,9	-	nd	nn	-18,8		333,2	
FI 63	37,1	22,7	8,6	5,5	8,1	-	nd	nn	-18,8		332,4	
FI 64	-	-	-	-	-	-	-	-	-		-	
FI 65	131,8	51,0	23,0	7,3	28,3	-	-	-	-18,8		332,1	
FI 66	-	-	-	-	-	-	-	-	-		-	
FI 67	-	-	-	-	-	-	-	-	-		-	
FI 68	-	-	-	-	-	-	-	-	-		-	
FI 69	-	-	-	-	-	-	-	-	-19,1		332,3	
FI 70	-	-	-	-	-	-	-	-	-		-	
FI 71	-	-	-	-	-	-	-	-	-18,5		329,5	
FI 72	-	-	-	-	-	-	-	-	-18,5		331,0	
FI 73	-	-	-	-	-	-	-	-	-		-	
FI 74	-	-	-	-	-	-	-	-25,6	-19,0	-19,0	333,2	
FI 75	-	-	-	-	-	-	-	-	-		-	
FI 76	274,5	72,9	31,4	11,1	57,1	-	nd	nn	-19,6		334,4	
FI 77	126,1	47,0	19,8	8,1	29,0	-	nd	nn	-19,5		333,4	
FI 78	193,9	51,3	19,0	13,0	45,1	-	nd	nn	-19,3		333,1	
FI 79	172,5	48,7	18,0	12,2	39,8	-	nd	nn	-20,2		334,3	
FI 80	128,0	57,1	27,4	5,9	25,0	-	nd	nn	-18,7		330,0	
FI 81	351,6	96,4	40,5	11,0	65,1	-	nd	nn	-19,5		333,6	
FI 82	162,3	52,7	18,5	11,2	32,2	-	nd	nn	-19,4		333,7	
FI 83	168,5	49,0	16,7	12,8	38,4	-	nd	nn	-18,9		331,4	
FI 84	-	-	-	-	-	-	nd	nn	-18,9		331,4	
FI 85	142,2	55,9	25,4	7,1	28,7	-	nd	nn	-18,9		333,2	
FI 86	60,0	28,4	10,3	7,4	12,9	-	nd	nn	-18,5		330,0	
FI 87	72,1	30,5	10,3	8,9	19,3	-	nd	nn	-19,0		330,3	
FI 88	76,9	33,5	13,2	7,4	21,2	-	nd	nn	-19,0		330,3	
FI 89	58,8	27,9	9,7	7,7	13,5	-	nd	nn	-18,9		331,4	
FI 90	128,0	42,3	16,0	10,2	30,6	-	nd	nn	-19,5		333,2	
FI 91	142,0	44,8	17,3	10,4	39,8	-	nd	nn	-19,4		332,9	
FI 92	108,0	38,5	14,4	9,5	28,8	-	nd	nn	-19,4		332,8	
FI 93	156,1	46,2	16,3	12,2	44,0	-	nd	nn	-19,5		333,2	
FI 94	49,4	25,3	8,2	7,6	12,6	-	nd	nn	-18,9		331,3	
FI 95	60,8	30,1	12,2	6,4	15,1	-	nd	nn	-19,2		330,7	
FI 96	3.798,8	261,4	100,6	48,1	725,0	-63,5	-23,8	-22,6	-18,0	-18,0	333,0	
FI 97	1.566,1	171,6	69,2	28,8	355,4	-64	-25,5	-23,7	-18,7	-18,3	334,0	
FI 98	193,6	52,4	19,6	12,6	39,6	-	nd	nn	-19,7		335,2	
FI 99	435,9	83,9	34,1	16,3	96,4	-	-	-24,5	-19,1		334,0	335,2
FI 100	720,3	136,7	54,5	16,8	157,6	-	nd	nn	-19,5		335,2	336,1

primary fluid inclusions

excluded data, or lost fluid inclusions after re-equilibration

Appendix A

GMR-005b

Inclusion	Depth / μm from Bottom/Top	from Side	magn.	Area μm^2	Perimeter μm	Best-Fit Ellips major (μm) minor (μm)		Area vapour μm^2	$T_c / ^\circ\text{C}$ SSV \rightarrow SLV	$T_m / ^\circ\text{C}$ SLV \rightarrow LV	$T_h / ^\circ\text{C}$ LV \rightarrow L
FI 1	100	25	100	577,7	90,2	33,7	21,9	159,7	-21,0	-16,9	324,8
FI 2	71	22	100	1370,2	162,8	61,1	28,5	321,1	-	-	330,4
FI 3	159	79	100	327,5	66,0	22,9	18,2	102,5	-	-	325,4
FI 4	156	65	100	53,4	26,8	9,3	7,3	13,7	-	-	325,3
FI 5	142	43	100	85,4	33,1	11,1	9,8	22,4	-	-	325,5
FI 6	110	25	100	106,9	37,4	13,0	10,5	34,2	-	-	319,2
FI 7	119	148	100	333,3	66,0	23,3	18,2	90,5	-	-	324,5
FI 8	161	128	100	149,4	44,7	15,9	12,0	48,1	-20,3	-	325,5
FI 9	161	130	100	322,9	65,7	23,3	17,7	84,1	-21,1	-	326,5
FI 10	160	112	100	68,1	30,7	11,4	7,6	21,8	-21,1	-16,5	328,9
FI 11	99	238	100	141,9	44,4	16,7	10,8	42,1	-	-	316,0
FI 12	80	227	100	42,9	25,1	10,0	5,4	10,2	-	-	274,5
FI 13	83	209	100	128,7	50,7	22,7	7,2	29,4	-	-	276,6
FI 14	94	256	100	213,9	54,3	18,3	14,9	59,6	-	-	274,0
FI 15	137	266	-----	-----	-----	-----	-----	-----	-	-	330,6
FI 16	54	407	100	244,7	56,8	18,9	16,5	77,2	-	-	287,8
FI 17	60	403	100	218,6	53,9	17,7	15,7	62,1	-	-	293,7
FI 18	128	389	100	79,2	32,4	11,7	8,6	24,0	-	-	327,5
FI 19	108	461	100	216,1	67,3	30,1	9,1	48,0	-	-	329,1
FI 20	63	443	100	72,1	31,6	12,0	7,6	19,5	-	-	319,0
FI 21	68	421	100	113,6	38,6	13,5	10,7	35,5	-	-	329,8
FI 22	49	378	40	110,7	38,1	13,5	10,4	34,9	-	-	329,0
FI 23	45	353	100	40,9	23,2	7,9	6,6	11,5	-	-	329,0
FI 24	49	378	100	44,3	24,2	8,6	6,5	10,4	-	-	329,0
FI 25	45	353	100	61,9	30,5	12,3	6,4	14,6	-	-	329,0
FI 26	79	403	100	315,0	92,7	38,5	10,4	55,6	-	-	328,5
FI 27	88	450	100	232,2	59,0	19,0	15,6	50,9	-	-	328,9
FI 28	45	288	pixel	58270,0	934,1	300,9	246,6	52,1	-	-	329,2
FI 29	54	263	40	235,1	59,2	19,1	15,6	52,1	-	-	329,0
FI 30	230	100	-----	-----	-----	-----	-----	-----	-	-	329,0
FI 31	17	173	100	155,3	45,8	17,0	11,6	39,3	-	-	329,0
FI 32	11	133	100	175,4	49,3	18,9	11,8	44,7	-	-	329,0
FI 33	40	104	100	122,0	42,2	17,0	9,2	28,6	-	-	329,0
FI 34	105	184	100	-----	-----	-----	-----	-----	-	-	329,8
FI 35	108	220	100	85,6	33,4	11,6	9,4	20,8	-	-	329,2
FI 36	144	353	100	84,8	36,1	14,9	7,2	17,8	-	-	329,1
FI 37	40	640,2	100	639,6	94,9	34,3	23,7	144,7	-	-	329,1
FI 38	123	382	40	640,2	95,1	34,4	23,7	142,5	-	-	267,0
FI 39	153	374	100	42,1	26,3	11,1	4,8	7,0	-	-	328,1
FI 40	162	346	100	156,0	50,0	18,4	10,8	32,2	-	-	316,6
FI 41	134	299	100	84,3	33,9	12,7	8,5	20,0	-	-	330,5
FI 42	139	371	100	75,0	32,3	12,4	7,7	20,6	-	-	327,5
FI 43	154	410	40	186,5	51,2	19,6	12,1	50,1	-	-	327,6
FI 44	140	443	100	465,9	79,0	27,9	21,2	132,4	-	-	327,6
FI 45	163	475	100	75,5	32,6	12,4	7,8	22,1	-	-	327,6
FI 46	37	392	40	277,0	60,0	20,2	17,4	84,1	-	-	327,9
FI 47	26	403	100	263,9	58,6	19,6	17,1	69,8	-	-	280,0
FI 48	148	338	100	428,8	84,8	35,0	15,6	109,7	-	-	279,0
FI 49	15	324	40	159,0	45,6	14,5	14,0	47,3	-	-	323,5
FI 50	17	317	100	157,7	45,5	14,4	13,9	40,8	-	-	325,1
FI 51	54	234	40	90,1	36,6	14,6	7,9	21,8	-	-	325,4
FI 52	54	234	40	939,5	148,0	46,1	25,9	183,5	-	-	325,0
FI 53	54	187	100	165,4	47,1	16,9	12,5	41,1	-	-	323,0
FI 54	26	133	100	794,7	121,0	50,8	19,9	147,7	-	-	275,9
FI 55	80	191	100	66,5	30,4	11,4	7,4	14,9	-	-	281,4
FI 56	133	144	100	177,6	57,3	24,7	9,2	37,9	-22,1	-16,5	319,8
FI 57	94	194	100	298,7	66,9	26,3	14,5	74,5	-	-	287,3
FI 58	20	655	40	1424,6	142,2	55,2	32,9	539,7	-	-	> 340,0
FI 59	11	637	40	298,7	66,9	26,3	14,5	74,5	-	-	326,8
FI 60	45	619	-----	-----	-----	-----	-----	-----	-	-	325,7
FI 61	31	619	100	69,1	30,4	10,8	8,1	18,8	-	-	328,3
FI 62	14	778	100	108,2	39,2	14,6	9,4	31,9	-	-	279,9
FI 63	46	479	-----	-----	-----	-----	-----	-----	-	-	322,6
FI 64	26	889	100	160,8	53,0	22,5	9,1	22,3	-	-	285,6
FI 65	37	972	100	509,4	84,8	32,2	20,2	144,0	-	-	289,0
FI 66	43	936	40	488,7	83,2	31,7	19,6	134,3	-	-	271,5
FI 67	29	994	100	613,8	63,5	21,7	18,4	73,3	-	-	289,4
FI 68	43	1030	100	139,2	67,6	34,2	5,2	32,8	-	-	278,9
FI 69	49	1102	40	1720,8	168,5	69,1	31,7	405,6	-	-	284,0
FI 70	40	1145	40	237,1	74,8	35,5	8,5	59,2	-	-	293,2
FI 71	22	1238	100	883,3	110,6	42,7	26,3	211,5	-	-	277,2
FI 72	51	1364	100	82,7	35,7	14,6	7,2	19,0	-	-	285,3
FI 73	66	1408	100	357,9	69,4	23,5	19,4	102,0	-	-	268,8
FI 74	48	1566	100	210,0	52,1	17,1	15,7	49,3	-	-	276,1
FI 75	130	677	100	50,4	25,9	9,1	7,1	14,5	-	-	322,2
FI 76	83	608	100	405,7	72,7	25,6	20,2	110,6	-	-	327,5
FI 77	77	569	100	192,7	50,1	16,6	14,7	50,1	-	-	328,4
FI 78	76	522	40	240,4	58,0	22,1	13,8	70,6	-	-	328,2
FI 79	88	551	100	248,5	58,9	22,5	14,0	68,6	-	-	312,1
FI 80	144	594	100	309,9	65,4	24,1	16,4	80,6	-	-	328,0
FI 81	148	745	100	56,8	28,3	10,4	6,9	12,2	-	-	284,0
FI 82	187	598	40	219,7	53,7	18,3	15,3	64,4	-	-	319,0
FI 83	117	443	100	330,4	68,3	26,2	16,1	83,3	-22,1	-17,1	329,2
FI 84	133	436	100	201,8	51,7	18,4	14,0	54,9	-	-	329,2
FI 85	40	1145	40	840,4	108,8	41,2	26,0	219,6	-	-	329,2
FI 86	127	479	100	216,4	53,1	16,9	16,3	67,6	-	-	329,0
FI 87	133	374	40	207,0	52,1	16,4	16,1	65,1	-22,1	-17,1	330,8
FI 88	127	328	100	201,2	53,8	20,8	12,3	60,9	-	-	329,1
FI 89	80	353	100	189,8	52,3	20,3	11,9	51,4	-	-	276,0
FI 90	46	277	100	250,6	101,4	36,6	8,7	47,0	-	-	284,5
FI 91	134	216	40	109,0	39,4	15,5	9,0	22,6	-	-	283,8
FI 92	149	83	100	158,5	46,5	15,5	13,0	48,1	-	-	328,6
FI 93	83	90	100	-----	-----	-----	-----	-----	-	-	327,2
FI 94	83	184	100	216,7	56,1	21,4	12,9	62,1	-21,2	-17,2	323,9
FI 95	74	216	100	86,5	33,8	11,9	9,2	23,2	-	-	324,6
FI 96	131	198	100	230,9	83,9	40,2	7,3	40,2	-	-	323,7
FI 97	145	169	100	129,6	44,8	18,4	9,0	27,7	-21,2	-17,2	325,5
FI 98	83	184	100	107,1	41,1	14,6	9,3	25,6	-	-	323,9
FI 99	117	72	100	-----	-----	-----	-----	-----	-	-	327,4
FI 100	108	115	100	106,2	41,3	17,4	7,8	26,8	-21,0	-16,6	327,1
FI 101	120	144	100	46,1	23,4	9,5	6,2	9,7	-	-	325,9
FI 102	117	360	100	33,8	21,5	7,6	5,7	6,3	-21,0	-	327,2
FI 103	96	389	100	38,9	26,0	11,2	4,4	10,0	-	-	327,6
FI 104	117	72	100	74,7	32,3	12,2	7,8	18,6	-	-	327,4
FI 105	108	115	100	65,2	32,7	14,0	5,9	15,3	-	-	327,1
FI 106	120	144	100	28,7	21,1	8,7	4,2	6,5	-	-	325,9
FI 107	117	360	100	61,2	30,8	12,9	6,0	12,8	-	-	327,2
FI 108	96	389	100	104,1	37,7	13,6	9,8	22,9	-	-	327,6

excluded data, inconsistent total homogenization temperatures

primary fluid inclusions

Eutectic temperature is varying between -22.1 and -20.3 °C, and may not correspond to the final dissolution temperature of hydrohalite at -21.1 °C
First recrystallisation during heating occurs at about - 22.1 °C, and can be mistaken for the eutectic temperature.

Appendix A

R-005b

Inclusion	Area µm ²	Perimeter µm	Best-Fit Ellips major (µm) minor (µm)		Area vapour µm ²	T _a / °C	T _{rest} / °C	T _m / °C hydrohalite	second T _m / °C hydrohalite	T _m / °C SLV → LV	second T _m / °C SLV → LV	T _v / °C LV → L	second T _v / °C LV → L	CO ₂ (1)	Raman (peak area) CO ₂ (2) N ₂		CH ₄
FI 1	601,8	91,1	33,8	22,6	168,6	-69	-29	-26,9	-27,0	-20,5	-20,6	334,4	334,0				
FI 2	1403,6	162,4	62,1	28,8	292,5	-67,5	-30	-26,7	-27,2	-20,4	-20,5	339,6	339,3				
FI 3	323,4	65,8	22,6	18,2	90,0	-68	-32	-29,0	-29,3	-20,7	-20,9	336,3	336,0				
FI 4	49,3	25,6	8,9	7,1	13,4	-70	nd	-	-	-21,6	-21,6	336,9					
FI 5	83,6	32,8	11,0	9,7	21,8	-70	-34	-	-30,4	-21,3	-21,4	337,0					
FI 6	98,3	35,9	12,5	10,0	26,6	-64	-27	-	-	-15,6	-15,6	327,6					
FI 7	333,7	65,8	23,1	18,4	83,0	-68	-29	-26,6	-26,6	-20,0	-19,9	333,2					
FI 8	147,2	44,2	15,7	12,0	43,4	-69	-32	-	-29,4	-20,8	-20,8	336,0					
FI 9	322,0	65,2	22,9	17,9	80,0	-	-	-27,4	-	-20,0	-	335,7					
FI 10	66,7	29,9	10,9	7,8	19,2	-	-	-	-	-21,0	-	339,9					
FI 11	141,7	44,4	16,7	11,0	39,8	-68,5	-34	-	-30,9	-22,0	-21,8	328,7					
FI 12	40,9	24,1	9,5	5,5	10,0	-41	-	-	-	-1,7	-	274,0	too deep	-	-	-	-
FI 13	130,7	50,2	22,3	7,5	31,8	-41	-	-	-	-1,6	-	275,1	too deep	-	-	-	-
FI 14	206,3	53,1	17,8	14,7	52,9	-41	-	-	-	-1,5	-	273,0	too deep	-	-	-	-
FI 15	-----					-72	nd	-	-	-22,0	-22,0	342,1					
FI 16	210,9	52,8	17,4	15,4	58,1	-41	-	-	-	-3,8	-1,9	-	286,6	too deep	-	-	-
FI 17	68,9	30,3	10,9	8,0	20,5	-	nd	-	-	-4,0	-1,8	-	292,7	too deep	-	-	-
FI 18	211,4	60,9	26,4	10,2	49,0	-69	-35	-	-30,8	-20,9	-20,9	338,2					
FI 19	69,2	30,9	11,8	7,5	16,6	-70,5	nd	-	-	-21,9	-21,8	340,3					
FI 20	-----					-71	-	-	-30,0	-21,9	-21,8	330,6					
FI 21	39,2	22,8	7,8	6,4	10,0	-65	nd	-31,0	-	-21,9	-22,1	341,1					
FI 22	40,6	23,1	8,1	6,4	10,6	-	-27,5	-	-	-22,1	-	340,6					
FI 23	56,5	29,5	11,9	6,0	13,0	-	nd	-	-	-22,2	-	340,6					
FI 24	268,2	65,0	26,8	12,8	51,4	-70	nd	-29,9	-29,6	-22,0	-21,8	338,3					
FI 25	229,7	57,9	18,6	15,7	51,4	-71,5	nd	-29,9	-30,0	-21,9	-21,7	340,1					
FI 26	-----					-	nd	-	-	-22,0	-	340,3					
FI 27	147,0	44,7	16,6	11,3	34,6	-70,5	nd	-	-30,0	-21,9	-21,9	340,1					
FI 28	159,1	46,6	17,6	11,5	40,6	-71,5	nd	-	-	-21,9	-21,8	340,1					
FI 29	171,1	41,1	16,5	9,1	27,1	-71	nd	-	-30,5	-21,9	-21,8	340,5					
FI 30	-----					-	-	-	-	-21,6	-	341,4					
FI 31	-----					-64	nd	-	-	-21,8	-	340,4					
FI 32	79,8	32,3	11,7	8,9	19,0	-71	nd	-	-33	-22,0	-22,0	340,4					
FI 33	81,2	35,1	14,4	7,2	17,5	-71,5	nd	-	-	-22,1	-22,0	340,5					
FI 34	623,6	91,2	32,7	24,3	136,0	-68	-31	-	-26,9	-20,6	-20,5	337,8					
FI 35	39,8	25,5	10,7	4,7	8,5	-41,5	nd	-	-	-	-1,6	-	267,6	too deep	-	-	-
FI 36	147,4	48,3	17,4	10,8	33,4	-	nd	-	-	-22,1	-	339,2					
FI 37	80,9	33,2	12,5	8,3	19,2	-	nd	-	-	-21,8	-21,9	328,9					
FI 38	74,5	32,1	12,0	7,9	18,5	-	nd	-	-	-21,3	-	340,6					
FI 39	179,1	50,1	19,3	11,8	44,9	-	nd	-27,4	-	-20,4	-	336,7					
FI 40	-----					-	nd	-26,6	-	-20,7	-	336,0					
FI 41	72,3	31,7	12,0	7,7	18,4	-68	nd	-	-28,3	-19,8	-21,1	337,2					
FI 42	254,2	57,3	19,0	17,0	73,0	-68	-32	-	-26,9	-20,4	-20,2	336,3					
FI 43	434,0	84,7	35,2	15,7	124,3	-40,5	-	-	-	-	-1,5	-	278,4	3095,29	5317,61	1875,82	0,00
FI 44	152,4	44,6	14,1	13,8	45,8	-	nd	-	-	-	-	-	277,5	2019,05	8192,00	1086,48	0,00
FI 45	85,8	35,5	14,2	7,7	21,7	-69	nd	-	-	-20,3	-20,3	333,7					
FI 46	-----					-	nd	-25,7	-	-19,2	-	332,5					
FI 47	163,1	46,1	16,0	13,0	46,6	-	nd	-26,3	-	-19,3	-	333,2					
FI 48	780,2	118,7	50,6	19,6	174,2	-64	-29	-25,4	-25,4	-19,8	-20,0	332,0					
FI 49	62,7	29,3	10,9	7,3	14,5	-65	nd	-	-	-21,9	-	334,8					
FI 50	150,9	50,0	21,0	9,2	40,3	-	-	-	-	-	-	-					
FI 51	-----					-	-	-	-	-	-	-					
FI 52	-----					-	-	-	-	-	-	-					
FI 53	-----					-	-	-	-	-	-	-					
FI 54	-----					-	-	-	-	-	-	-					
FI 55	-----					-	-	-	-	-	-	-					
FI 56	68,4	30,1	10,3	8,5	17,0	-71	nd	-	-	-21,8	-	336,8					
FI 57	69,8	30,4	10,8	8,2	20,1	-	-	-	-	-21,9	-	339,4					
FI 58	-----					-	-	-	-	-	-	-					
FI 59	-----					-	-	-	-	-20,3	-	331,5					
FI 60	161,1	52,5	22,3	9,2	40,6	-41	-	-	-	-	-1,4	-	284,1	1804,74	2628,97	1552,91	867,38
FI 61	481,9	82,4	31,4	19,5	127,3	-	-	-	-	-	-	287,4					
FI 62	312,2	63,5	21,4	18,5	73,0	-	-	-	-	-	-	269,8	1532,45	2920,85	1563,10	1627,88	
FI 63	137,7	66,8	33,6	5,2	31,2	-	-	-	-	-	-	288,2	2023,12	3285,14	1750,65	7150,65	
FI 64	-----					-41	-	-	-	-	-1,4	-	277,2	642,18	1163,74	838,20	2600,82
FI 65	224,0	72,7	34,6	8,2	57,7	-	-	-	-	-	-	282,6	1770,24	3396,89	1471,65	6578,61	
FI 66	871,0	109,9	42,5	26,1	262,7	-	-	-	-	-	-	291,8	2390,11	4658,73	2474,37	33106,60	
FI 67	78,0	34,4	14,0	7,1	18,4	-	-	-	-	-	-	275,7	1687,15	4212,51	1425,12	2392,05	
FI 68	349,7	68,6	23,3	19,1	98,4	-40,5	-	-	-	-	-1,3	-	283,8	2056,03	3782,63	1844,07	14675,80
FI 69	205,3	51,4	17,0	15,4	47,4	-	-	-	-	-	-	267,0	1545,46	2313,84	1433,18	3525,27	
FI 70	48,4	25,2	8,7	7,0	12,0	-	-	-	-	-	-	275,2					
FI 71	397,5	72,1	25,6	19,7	96,7	-66,5	-29	-	-26,6	-19,8	-19,8	330,3					
FI 72	184,8	49,0	16,3	14,4	48,5	-70,5	-33	-	-29,4	-21,7	-21,7	338,0					
FI 73	238,0	57,9	22,1	13,7	52,7	-70	-32	-	-28,7	-21,5	-21,4	338,9					
FI 74	304,3	64,8	23,9	16,2	74,1	-	-	-26,5	-	-20,2	-	336,0					
FI 75	54,7	27,7	10,2	6,8	10,6	-	-	-	-	-	-	325,0					
FI 76	214,2	53,3	18,2	15,0	57,2	-69	-33	-	-28,8	-21,3	-21,2	338,1					
FI 77	323,3	67,4	25,6	16,1	85,0	-	-	-	-	-	-	283,0	753,34	1076,94	897,62	4015,02	
FI 78	188,1	49,7	17,5	13,7	45,4	-68	-33	-	-28,4	-20,5	-20,4	328,7					
FI 79	845,9	109,0	40,4	26,9	206,4	-	-30	-	-25,2	-20,0	-20,1	336,8					
FI 80	204,5	51,9	16,2	16,1	54,4	-69,5	-33	-	-27,9	-21,0	-21,0	338,4					
FI 81	190,2	51,9	19,9	12,2	46,3	-	-33	-	-27,0	-20,5	-20,6	337,6					
FI 82	242,3	84,9	32,7	9,4	50,0	-	-35	-	-29,6	-21,9	-21,8	341,6					
FI 83	108,0	39,1	15,3	9,0	22,4	-69,5	nd	-	-	-22,0	-21,8	340,3					
FI 84	165,6	46,9	15,4	13,7	42,7	-	-	-	-	-	-	-	275,1				
FI 85	-----					-	-	-	-	-	-	-	-				
FI 86	-----					-	-	-	-	-	-	-	-				
FI 87	-----					-69	nd	-	-	-21,8	-21,7	341,5					
FI 88	-----					-71,5	nd	-	-	-21,9	-21,8	341,3					
FI 89	127,8	44,4	18,2	9,0	27,5	-	nd	-	-30,0	-21,9	-21,9	341,4					
FI 90	108,8	41,0	14,5	9,5	25,6	-	nd	-	-	-21,9	-21,9	341,4					
FI 91	-----					-	-	-	-	-	-	-					
FI 92	98,5	39,4	16,4	7,6	26,0	-	nd	-	-	-19,5	-19,8	-					
FI 93	44,5	24,9	9,4	6,0	9,5	-71,5	nd	-	-	-20,8	-21,3	335,1					
FI 94	32,6	21,0	7,4	5,6	6,3	-	nd	-	-30,3	-21,7	-21,4	335,7					
FI 95	39,2																

Appendix A

GMR-005c										R-005c							
Inclusion	Depth / μm from Bottom/Top	from Side	Area (pixel) ²	Perimeter (pixel) ²	Best-Fit Ellips Major axis		T_p / °C SSV \rightarrow SLV	T_{ph} / °C SLV \rightarrow LV	T_p / °C LV \rightarrow L	Inclusion	T_p / °C	T_{ph} / °C	T_{ph} / °C hydrohalite	T_p / °C SLV \rightarrow LV	second T_{ph} / °C SLV \rightarrow LV	T_p / °C LV \rightarrow L	second T_p / °C LV \rightarrow L
F11	233	245	171719	2694	1219	179	# -21,5	-16,5	330,3	F11	-62,5	-26,0	-23,9	-17,7	-18,0	330,8	330,0
F12	117	418	36604	929	425	110	-	-	330,1	F12	-	-	-	-17,8	-	329,7	-
F13	179	209	38472	884	401	122	-	-	329,8	F13	-	-	-	-17,1	-	329,9	-
F14	184	119	25222	642	272	118	-	-	331,0	F14	-	-	-	-	-	330,7	-
F15	205	158	17797	500	195	116	-	-	330,1	F15	-	-	-	-	-	329,6	-
F16	230	108	52894	1852	635	106	-	-	332,1	F16	-	-	-	-16,9	-	328,6	-
F17	241	76	30304	1214	538	72	-	-	331,7	F17	-	-	-	-	-	328,6	-
F18	221	130	21440	565	219	125	-	-	328,9	F18	-66,0	-	-25,5	-18,0	-18,3	328,8	327,8
F19	179	281	28011	614	209	171	-	-	331,2	F19	-	-	-	-18,1	-18,4	332,4	331,5
F110	-	-	65968	1168	516	163	-	-	-	F110	-65,0	-24,3	-23,5	-	-18,3	-	331,7
F111	96	281	37403	744	291	164	-	-	331,6	F111	-58,0	-26,4	-24,5	-17,5	-17,8	330,7	330,0
F112	62	374	100160	1810	418	305	-	-	331,7	F112	-61,0	-28,0	-24,3	-17,3	-17,9	331,1	330,3
F113	90	346	18334	495	182	129	-	-	331,0	F113	-65,0	-	nd	-17,7	-17,8	329,4	328,6
F114	90	317	17735	491	177	128	-	-	330,6	F114	-63,5	-	nd	-17,4	-17,6	328,3	327,4
F115	93	295	53536	904	362	188	-	-	331,4	F115	-64,5	-27,5	-24,4	-18,1	-18,1	331,5	330,7
F116	90	241	16266	470	161	129	-	-	331,2	F116	-65,0	-27,0	-25,6	-17,5	-17,7	329,0	328,2
F117	80	209	11292	424	178	81	-	-	328,0	F117	-65,0	-	nd	-17,5	-17,7	326,2	325,5
F118	80	184	12179	443	188	82	-	-	329,2	F118	-63,0	-	-26,0	-16,3	-16,6	324,4	323,5
F119	90	176	15953	503	212	96	-	-	326,8	F119	-65,0	-28,0	-25,9	-17,1	-17,2	323,7	323,0
F120	102	148	19816	576	246	102	-	-	327,5	F120	-	-	nd	-16,6	-16,6	321,2	320,5
F121	114	72	30349	664	264	146	-	-	328,6	F121	-66,5	-26,5	-24,8	-18,1	-18,3	328,8	328,3
F122	114	50	33456	726	289	148	-	-	329,3	F122	-64,5	-27,0	-24,9	-18,1	-18,3	329,6	328,9
F123	102	50	17056	499	195	111	-	-	330,7	F123	-65,5	-	-25,8	-17,5	-17,6	327,7	327,2
F124	71	36	38505	956	430	114	-	-	331,8	F124	-63,0	-	nd	-17,5	-17,7	329,8	329,2
F125	71	79	12383	400	136	116	-	-	327,9	F125	-65,0	-	-25,7	-17,5	-17,7	325,0	-
F126	102	83	18625	521	204	116	-	-	328,2	F126	-	-	nd	-17,9	-18,0	327,0	-
F127	96	162	21118	538	201	134	-	-	328,0	F127	-	-	-	-17,9	-	327,8	-
F128	111	151	51730	1371	614	107	-	-	327,5	F128	-66,0	-28,0	-25,0	-17,8	-18,1	328,2	-
F129	128	148	19352	609	276	89	-	-	328,1	F129	-	-	-	-17,3	-	325,9	-
F130	117	43	82355	1789	821	128	-	-	328,6	F130	-	-	-	-17,4	-	327,0	-
F131	117	61	29959	630	222	172	-	-	330,3	F131	-65,0	-	nd	-17,7	-18,0	328,8	-
F132	-	-	24619	784	369	85	-	-	-	F132	-	-	-	-	-	-	-
F133	97	25	13777	446	174	101	-	-	328,8	F133	-	-	nd	-17,0	-17,3	326,6	-
F134	97	112	20369	536	206	126	-	-	327,3	F134	-64,5	-	nd	-17,7	-18,0	325,9	-
F135	105	158	19834	520	196	129	-	-	327,6	F135	-64,0	-	-26,3	-16,9	-17,1	323,4	-
F136	105	158	18307	531	219	107	-	-	327,5	F136	-65,5	-	-25,4	-17,7	-17,9	326,2	-
F137	114	205	16406	467	158	132	-	-	327,5	F137	-65,0	-	-25,2	-17,6	-17,7	325,8	-
F138	114	230	19212	533	214	115	-	-	327,8	F138	-62,0	-	nd	-17,6	-17,8	325,8	-
F139	114	230	17661	479	166	135	-	-	327,9	F139	-66,0	-	nd	-17,6	-17,9	326,3	-
F140	113	166	15905	468	179	113	-	-	326,9	F140	-64,0	-	-24,9	-17,6	-17,7	325,2	-
F141	230	36	23354	603	245	121	-	-	321,5	F141	-63,5	-	nd	-16,0	-16,1	319,7	-
F142	230	94	17175	495	195	112	-	-	321,5	F142	-60,0	-	-25,0	-16,6	-16,2	319,7	-
F143	233	166	26137	630	256	130	-	-	324,5	F143	-63,5	-	-24,2	-16,6	-16,6	324,7	-
F144	221	151	25521	608	230	141	-	-	326,9	F144	-	-	-	-15,9	-	325,1	-
F145	185	32	63566	1684	736	110	-	-	327,8	F145	-	-	-	-14,5	-	320,8	-
F146	197	220	34456	844	390	112	-	-	327,9	F146	-	-	-	-16,0	-	327,0	-
F147	245	277	29141	712	311	119	-	-	328,0	F147	-	-	-	-16,0	-16,3	327,8	-
F148	253	360	39122	909	424	118	-	-	328,9	F148	-	-	-	-16,0	-	326,8	-
F149	236	346	17887	543	231	99	-	-	328,9	F149	-	-	-	-15,7	-	325,1	-
F150	174	342	25191	579	209	154	-	-	328,0	F150	-	-	-	-15,8	-	326,5	-
F151	11	220	20761	591	246	108	-	-	330,1	F151	-	-	-	-17,3	-	326,5	-
F152	31	274	19418	613	277	89	-	-	330,5	F152	-	-	-	-17,3	-	327,5	-
F153	48	320	18124	717	354	65	-	-	330,0	F153	-	-	-	-17,3	-	325,4	-
F154	49	356	16742	467	162	131	-	-	327,8	F154	-64,0	-	25,0	-16,8	-17,0	323,6	-
F155	20	414	10347	370	131	101	-	-	330,7	F155	-	-	-	-	-16,4	325,3	-
F156	15	83	14287	546	255	71	-	-	-	F156	-	-	-	-	-	-	-
F157	15	97	15982	480	188	108	-	-	325,3	F157	-64,0	-	nd	-17,1	-17,3	323,2	322,0
F158	19	223	21460	987	503	54	-	-	329,6	F158	-63,0	-	-25,5	-17,2	-17,3	327,8	326,9
F159	19	194	9633	416	186	66	-	-	326,5	F159	-	-	-25,8	-17,3	-17,3	324,4	323,5
F160	25	313	34022	1067	539	80	-	-	327,2	F160	-62,0	-	-25,7	-16,0	-16,6	323,7	322,7
F161	29	252	22157	725	334	84	-	-	329,6	F161	-63,0	-26,0	-24,8	-17,4	-17,5	329,2	328,3
F162	43	288	36074	793	318	144	-	-	329,7	F162	-65,5	-27,0	-24,6	-17,4	-17,7	330,2	329,1
F163	52	248	18480	537	223	105	-	-	325,7	F163	-63,5	-	-25,0	-16,9	-17,0	323,3	322,6
F164	153	274	10128	381	150	86	-	-	328,1	F164	-63,5	-	-25,6	-16,8	-17,1	325,7	324,6
F165	153	259	10833	400	162	85	-	-	326,2	F165	-65,0	-	-25,0	-17,4	-17,8	326,5	325,5
F166	164	223	14403	448	164	112	-	-	325,0	F166	-64,5	-	-	-17,4	-17,5	324,6	323,6
F167	171	191	22106	596	252	112	-	-	327,2	F167	-	-	-	-17,4	-17,6	326,6	325,3
F168	182	122	19295	569	242	101	-	-	323,3	F168	-	-	-	-17,4	-	323,2	322,0
F169	188	104	12190	578	283	55	-	-	321,7	F169	-	-	-	-17,1	-	322,0	-
F170	188	119	7522	317	107	89	-	-	322,0	F170	-	-	-	-16,8	-	319,6	-

(pixel)² 1 μm = 15,83 pixel

-25,0 uncertain numbers

Eutectic temperature is varying between -21,5 and -21,1 $^\circ\text{C}$, and may not correspond to the final dissolution temperature of hydrohalite at -21,1 $^\circ\text{C}$. First recrystallisation during heating occurs at about - 21,5 $^\circ\text{C}$, and can be mistaken for the eutectic temperature.

excluded data, lost fluid inclusions after re-equilibration

calibration difficulties:

the average difference of second measurement is 0,2 $^\circ\text{C}$ lower for T_m
the average difference of second measurement is 0,9 $^\circ\text{C}$ lower for T_h

Appendix A

GMR-011a										R-011a				
Inclusion	Depth / μm		Area (pixel)*	Perimeter (pixel)*	Best-Fit Ellips		$T_e / ^\circ\text{C}$		$T_m / ^\circ\text{C}$ SLV \rightarrow LV	$T_h / ^\circ\text{C}$ LV \rightarrow L	Inclusion	$T_m / ^\circ\text{C}$ hydrohalite	$T_m / ^\circ\text{C}$ SLV \rightarrow LV	$T_h / ^\circ\text{C}$ LV \rightarrow L
	from Bottom	from Top			Major axis	Minor axis	SSV	SLV						
F1	157	76	340613	2272	894	485	-	-	-	316,4	F1	-	-7,3	314,4
F2	176	112	-	-	-	-	-21,1	-6,6	-	318,8	F2	-	-7,4	312,8
F3	218	176	20850	562	215	123	-	-	-	313,7	F3	-	-7,3	312,1
F4	256	241	180625	2901	1345	171	-21,1	-6,5	-	314,5	F4	-	-7,4	312,9
F5	238	227	123397	1466	582	270	-21,1	-6,6	-	314,2	F5	-	-7,5	312,7
F6	252	360	87965	1664	743	151	-	-	-	313,4	F6	-	-7,4	312,1
F7	174	346	36139	832	379	122	-	-	-	314,3	F7	-	-6,8	312,8
F8	185	349	37463	849	386	123	-	-	-	313,9	F8	-	-6,8	312,5
F9	219	353	24374	569	196	158	-	-	-	313,9	F9	-	-7,4	311,9
F10	219	385	27804	653	264	134	-	-	-	313,9	F10	-	-7,5	311,9
F11	219	367	32049	669	251	162	-	-	-	314,9	F11	-	-7,3	313,1
F12	108	446	20263	545	206	125	-	-	-	313,6	F12	-	-7,3	311,6
F13	88	479	30281	746	331	116	-	-	-	314,2	F13	-	-7,4	312,2
F14	71	400	28585	999	414	88	-	-	-	314,1	F14	-	-7,4	312,3
F15	59	403	22376	604	252	113	-	-	-	313,9	F15	-	-7,4	311,8
F16	80	446	30558	680	279	140	-	-	-	313,8	F16	-	-7,4	312,4
F17	137	482	50119	871	350	182	-	-	-	314,0	F17	-	-7,5	312,1
F18	62	515	69830	1035	406	219	-	-	-	314,1	F18	-	-7,4	314,5
F19	91	814	189208	1714	579	416	-21,1	-6,6	-	316,0	F19	-	-7,2	312,1
F20	177	1012	67696	948	343	252	-	-	-	313,6	F20	-	-7,2	311,0
F21	201	976	38178	731	269	181	-21,1	-6,6	-	312,6	F21	-	-7,1	311,4
F22	225	936	189906	2805	1072	225	-	-	-	312,2	F22	-	-7,2	311,4
F23	125	1087	380675	2298	859	564	-	-	-	312,5	F23	-	-7,2	311,4
F24	142	1008	-	-	-	-	-21,1	-6,6	-	312,2	F24	-	-	311,4
F25	256	868	40056	758	298	171	-	-	-	314,0	F25	-	-7,4	312,7
F26	241	835	39402	749	288	174	-	-	-	313,9	F26	-	-7,3	312,2
F27	241	889	20714	522	167	158	-	-	-	313,9	F27	-	-7,3	311,9
F28	253	821	55195	886	339	207	-	-	-	313,2	F28	-	-7,4	312,1
F29	253	0	37972	893	415	116	-	-	-	313,6	F29	-	-7,3	311,9
F30	253	785	13784	448	178	99	-	-	-	313,6	F30	-	-7,3	312,6
F31	253	774	78613	1279	549	182	-	-	-	313,9	F31	-	-7,3	312,6
F32	239	727	165194	2389	978	215	-	-6,7	-	313,7	F32	-	-7,3	312,6
F33	236	677	122375	2861	1185	131	-	-	-	313,7	F33	-	-7,2	312,6
F34	227	785	59038	1076	487	154	-	-6,7	-	314,7	F34	-	-7,2	313,4
F35	250	688	16922	559	241	89	-	-	-	314,7	F35	-	-7,3	312,4
F36	241	698	27735	635	231	153	-	-	-	313,8	F36	-	-7,3	311,9
F37	253	691	20166	533	206	125	-	-	-	313,7	F37	-	-7,2	311,7
F38	249	709	25011	626	260	122	-	-	-	313,8	F38	-	-7,1	312,0
F39	196	803	27478	645	265	132	-	-	-	314,0	F39	-	-7,3	312,4
F40	224	713	29223	657	263	141	-	-	-	314,1	F40	-	-7,3	312,4
F41	252	713	18737	512	184	130	-	-	-	314,0	F41	-	-7,3	312,4
F42	239	691	92338	1377	400	294	-	-	-	313,9	F42	-	-7,1	312,8
F43	239	587	78113	1138	472	211	-	-	-	313,6	F43	-	-7,1	312,2
F44	207	306	336431	4228	1245	344	-21,1	-6,6	-	314,0	F44	-	-7,1	312,6
F45	207	396	39692	730	257	197	-	-	-	313,9	F45	-	-7,1	312,4
F46	221	277	62677	1149	415	192	-	-	-	313,2	F46	-	-7,1	313,1
F47	248	202	58854	901	337	222	-	-	-	313,7	F47	-	-7,3	312,3
F48	221	83	43513	797	304	182	-	-	-	313,7	F48	-	-7,2	312,4
F49	176	317	48176	805	272	226	-	-	-	313,8	F49	-	-7,1	312,2
F50	199	353	44844	845	354	161	-	-	-	313,9	F50	-	-7,2	312,3
F51	199	310	33339	694	255	167	-	-	-	313,9	F51	-	-7,2	312,2
F52	173	43	34565	694	252	174	-	-	-	-	F52	-	-7,3	-
F53	253	576	86971	1133	443	250	-	-	-	314,1	F53	-	-7,3	312,9
F54	239	486	40005	722	240	212	-	-	-	314,1	F54	-	-7,3	312,5
F55	208	490	38436	785	333	147	-	-	-	314,1	F55	-	-7,3	312,4
F56	228	353	43082	770	288	190	-	-	-	313,8	F56	-	-7,1	312,4
F57	198	302	53565	892	352	194	-	-	-	314,1	F57	-	-7,3	313,1
F58	242	241	25930	619	250	132	-	-	-	313,6	F58	-	-7,2	312,0
F59	239	209	21492	580	242	113	-	-	-	313,6	F59	-	-7,3	312,0
F60	205	205	37050	733	268	176	-	-	-	314,2	F60	-	-7,4	312,6
F61	204	122	31530	659	218	184	-	-	-	314,4	F61	-	-7,3	312,7
F62	219	137	21039	556	223	120	-	-	-	313,9	F62	-	-7,2	312,2
F63	228	126	108295	2191	777	177	-	-	-	314,3	F63	-	-7,1	312,8
F64	191	158	56404	924	378	190	-	-	-	314,3	F64	-	-7,3	312,6
F65	247	72	56866	923	353	205	-	-	-	314,4	F65	-	-7,4	313,2
F66	188	148	30841	888	213	184	-	-	-	313,8	F66	-	-7,2	312,0
F67	211	115	38425	734	274	179	-	-	-	313,9	F67	-	-7,2	312,4
F68	177	191	22802	596	247	117	-	-	-	313,8	F68	-	-7,3	312,0
F69	208	50	17247	532	222	99	-	-	-	313,2	F69	-	-7,3	311,8
F70	167	47	33935	766	334	129	-	-	-	313,6	F70	-	-7,3	312,3
F71	136	68	38080	1416	673	72	-	-	-	313,8	F71	-	-7,3	312,4
F72	134	25	35940	688	245	186	-	-	-	313,6	F72	-	-7,3	312,4
F73	111	72	17232	683	175	125	-	-	-	313,6	F73	-	-7,2	312,1
F74	105	130	67758	1312	606	142	-	-	-	311,8	F74	-	-7,3	310,7
F75	148	205	23375	581	230	129	-	-	-	313,7	F75	-	-7,3	312,1
F76	93	227	66210	1129	501	168	-	-6,6	-	314,1	F76	-	-7,3	313,2
F77	59	238	28682	665	258	142	-	-6,6	-	313,8	F77	-	-7,2	312,2
F78	26	248	25083	799	381	84	-	-6,6	-	313,7	F78	-	-7,3	312,3
F79	54	349	33717	1009	502	86	-	-	-	314,4	F79	-	-7,1	312,9
F80	86	482	34559	703	279	157	-	-	-	314,1	F80	-	-7,1	312,4
F81	105	468	111577	1340	564	252	-	-	-	314,1	F81	-	-7,1	312,6
F82	161	490	85792	1131	434	252	-21,1	-6,6	-	313,5	F82	-	-7,1	312,4
F83	161	540	71307	1029	401	226	-21,1	-6,6	-	313,5	F83	-	-7,1	312,4
F84	94	580	30563	685	264	148	-	-	-	314,1	F84	-	-7,3	312,3
F85	151	598	26469	698	314	107	-	-	-	313,5	F85	-	-7,3	312,1
F86	193	558	34891	798	355	125	-	-	-	315,1	F86	-	-7,3	313,7
F87	174	680	198919	3522	959	264	-	-6,6	-	313,3	F87	-	-6,9	311,8
F88	179	544	39169	753	281	177	-	-	-	313,5	F88	-	-7,1	312,2
F89	174	526	38861	731	275	180	-	-	-	313,6	F89	-	-7,1	312,4
F90	-	256	31815	662	236	172	-	-	-	-	F90	-	-	-
F91	51	414	34059	742	294	148	-	-	-	313,5	F91	-	-7,0	312,3
F92	70	450	36978	952	449	105	-	-	-	313,5	F92	-	-7,0	312,6
F93	120	490	45229	903	338	171	-	-	-	313,4	F93	-	-7,1	312,3
F94	124	439	33845	678	225	192	-	-	-	314,2	F94	-	-7,1	312,3
F95	137	425	17274	531	222	99	-	-	-	313,2	F95	-	-7,0	311,5
F96	252	533	19836	769	376	67	-	-	-	312,9	F96	-	-7,3	311,7
F97	252	670	27227	703	312	111	-	-	-	313,5	F97	-	-7,2	313,2

(pixel)* 1 μm = 15,83 pixel

excluded data, lost fluid inclusions after re-equilibration

Appendix A

GMR-014a										R-014a			
Inclusion	Depth / μm		Area (pixel)*	Perimeter (pixel)*	Best-Fit Ellips		$T_p / ^\circ\text{C}$	$T_m / ^\circ\text{C}$	$T_b / ^\circ\text{C}$	Inclusion	$T_m / ^\circ\text{C}$	$T_p / ^\circ\text{C}$	$T_b / ^\circ\text{C}$
	from Top	from Side			Major axis	Minor axis	SSV \rightarrow SLV	SLV \rightarrow LV	LV \rightarrow L		hydrohalite	SLV \rightarrow LV	LV \rightarrow L
FI1	31	212	102894	2280	1008	130	-	-	328,5	FI1	-	-16,0	335,3
FI2	40	270	35617	1046	455	100	-	-	329,9	FI2	-	-16,3	335,8
FI3	40	274	11084	393	140	101	-	-	324,8	FI3	-	-16,3	331,9
FI4	40	238	16080	588	268	76	-	-	330,9	FI4	-	-16,3	337,3
FI5	49	223	6349	314	128	63	-	-	329,9	FI5	-	-16,4	336,0
FI6	88	198	83961	1272	379	282	-	-	328,8	FI6	-	-16,1	335,6
FI7	22	61	25495	574	184	177	-	-	330,4	FI7	-	-16,2	336,9
FI8	43	40	16046	455	154	132	-	-	328,3	FI8	-	-16,3	335,0
FI9	43	7	21274	605	216	125	-	-	328,9	FI9	-	-16,2	335,2
FI10	88	234	11307	540	261	55	-	-	328,0	FI10	-	-16,4	334,7
FI11	49	259	104778	1659	644	207	-	-12,4	328,7	FI11	-	-16,4	336,0
FI12	35	320	28013	639	236	151	-	-12,4	330,1	FI12	-	-16,5	336,8
FI13	40	313	19650	508	178	141	-	-12,4	329,1	FI13	-	-16,5	336,0
FI14	11	346	14803	461	170	111	-	-	329,1	FI14	-	-16,5	336,0
FI15	23	353	11050	393	131	107	-	-	329,9	FI15	-	-16,5	335,9
FI16	11	346	15684	497	205	97	-	-	329,7	FI16	-	-16,5	336,2
FI17	11	360	13270	495	179	94	-	-	328,7	FI17	-	-16,5	334,7
FI18	23	331	16798	548	198	108	-	-	328,5	FI18	-	-16,5	334,9
FI19	35	403	20166	551	221	116	-	-	329,5	FI19	-	-16,5	334,7
FI20	28	288	19428	596	254	98	-	-	328,9	FI20	-	-16,5	335,4
FI21	145	198	42864	903	393	139	-	-	328,5	FI21	-	-16,5	336,0
FI22	177	256	47938	825	289	211	-	-	328,0	FI22	-	-16,3	335,0
FI23	163	266	33218	746	317	134	-	-	327,8	FI23	-	-16,3	335,4
FI24	128	367	18993	559	237	102	-	-	327,8	FI24	-	-16,3	335,7
FI25	154	482	19187	608	266	92	-	-	327,8	FI25	-	-16,4	335,3
FI26	128	475	42904	810	329	166	-	-	329,0	FI26	-	-15,7	336,3
FI27	126	482	40242	846	373	137	-	-	327,9	FI27	-	-15,8	336,0
FI28	57	518	17078	495	194	112	-	-	328,8	FI28	-	-16,3	336,3
FI29	142	608	29711	791	355	107	-	-	328,0	FI29	-	-16,4	335,6
FI30	184	558	19937	573	242	105	-	-	329,9	FI30	-	-16,4	337,4
FI31	120	166	20162	566	234	110	-	-	329,5	FI31	-	-15,9	336,9
FI32	150	230	35843	769	322	142	-	-	328,2	FI32	-	-15,5	335,5
FI33	165	317	39335	1222	549	91	-	-	325,3	FI33	-	-15,7	332,0
FI34	134	302	73494	1827	701	133	-	-	327,4	FI34	-	-15,8	333,6
FI35	89	230	24989	616	233	137	-	-	327,4	FI35	-	-15,9	335,0
FI36	62	97	29277	649	245	152	-	-	329,3	FI36	-	-	-
FI37	62	299	31873	667	232	175	-	-	327,5	FI37	-	-	-
FI38	65	468	56124	1680	586	122	-	-	328,1	FI38	-	-15,8	334,0
FI39	65	522	14984	466	179	107	-	-	330,4	FI39	-	-15,9	335,8
FI40	65	619	24090	719	333	92	-	-	328,1	FI40	-	-15,9	335,3
FI41	154	173	31103	788	351	113	-	-	328,4	FI41	-	-15,2	335,4
FI42	20	306	20905	591	232	115	-	-	328,0	FI42	-	-15,7	335,2
FI43	25	295	11761	406	128	117	-	-	328,9	FI43	-	-15,8	336,0
FI44	26	263	13909	603	208	85	-	-	324,9	FI44	-	-16,0	331,8
FI45	25	295	14620	458	161	116	-	-	328,4	FI45	-	-15,9	335,2
FI46	6	263	111403	1342	520	273	-	-	330,0	FI46	-	-	-
FI47	31	151	26991	835	296	116	-	-	328,3	FI47	-	-16,1	335,2
FI48	97	50	33251	759	269	158	-	-	328,0	FI48	-	-15,7	335,0
FI49	88	76	39467	761	234	215	-	-	328,3	FI49	-	-15,8	335,2
FI50	97	104	23286	589	234	127	-	-	328,0	FI50	-	-15,9	335,0
FI51	82	194	93629	1376	618	193	-	-12,4	328,9	FI51	-	-15,5	335,4
FI52	59	230	92625	1156	438	269	-	-12,4	330,4	FI52	-	-15,5	337,0
FI53	8	302	229181	3023	1004	291	-	-	329,7	FI53	-	-14,0	336,5
FI54	85	234	57081	882	292	249	-	-	329,5	FI54	-	-15,5	336,2
FI55	28	90	23075	674	287	102	-	-	330,9	FI55	-	-15,9	337,2
FI56	125	47	23700	581	215	140	-	-	328,0	FI56	-	-15,3	334,9
FI57	103	94	22304	797	299	95	-	-	325,2	FI57	-	-15,9	332,2
FI58	88	130	24478	625	246	127	-	-	329,6	FI58	-	-15,9	336,3
FI59	43	58	21513	591	247	111	-	-	329,9	FI59	-	-16,0	336,6
FI60	91	162	20890	580	245	108	-	-	329,5	FI60	-	-16,0	336,0
FI61	14	205	14802	480	200	94	-	-	326,6	FI61	-	-15,7	333,0
FI62	40	162	12396	413	154	102	-	-	327,8	FI62	-	-15,8	334,6
FI63	43	47	13991	448	170	105	-	-	327,3	FI63	-	-16,4	334,1
FI64	12	58	7852	336	126	79	-	-	327,4	FI64	-	-16,3	333,7
FI65	9	115	6515	306	117	71	-	-	328,7	FI65	-	-	-
FI66	130	252	19913	572	244	104	-	-	331,9	FI66	-	-16,2	338,4
FI67	119	223	8258	332	119	88	-	-	326,1	FI67	-	-16,4	333,4
FI68	69	72	10777	394	154	89	-	-	328,2	FI68	-	-16,3	335,0
FI69	48	169	15902	561	227	89	-	-	328,1	FI69	-	-16,3	334,5
FI70	54	137	45034	1363	545	105	-	-	328,3	FI70	-	-16,1	334,8
FI71	56	126	12630	495	214	75	-	-	328,2	FI71	-	-16,0	334,2

(pixel)* 1 μm = 15,83 pixel

excluded data, lost fluid inclusions after re-equilibration